Active Combustion Control: Modeling, Design and Implementation

by

Sungbae Park

M.S., Mechanical Engineering
Massachusetts Institute of Technology, 2001

Submitted to the Department of Mechanical Engineering
in Partial Fulfillment of the Requirements for the Degree of

Doctor of Philosophy

at the

Massachusetts Institute of Technology

June 2004

Signature of Author .....
Department of Mechanical Engineering
May 7, 2004

Certified by .....
Anuradha M. Annaswamy
Senior Research Scientist
Thesis Supervisor

Certified by .....
Ahmed F. Ghoniem
Professor
Thesis Supervisor

Accepted by .....
Ain A. Sonin
Chairman, Department Committee on Graduate Students

Active Combustion Control: Modeling, Design and Implementation

by

Sungbae Park

Submitted to the Department of Mechanical Engineering
on May 7, 2004, in Partial Fulfillment of the
Requirements for the Degree of
Doctor of Philosophy in Mechanical Engineering

Abstract

Continuous combustion systems common in propulsion and power generation applications are susceptible to thermoacoustic instability, which occurs under lean burn conditions close to the flammability where most emissions and efficiency benefits are achieved, and near stoichiometry where often high power density can be realized. This instability is undesirable because the accompanying large pressure and heat release rate oscillations lead to high levels of acoustic noise and vibration as well as structural damage. Active control is one approach using which such instabilities can be mitigated. Over the past five to ten years, it has been shown conclusively through several lab-scale studies that active control is highly successful in suppressing the pressure oscillations. This success has set the stage for transition of the technology from laboratories to large-scale applications in propulsion and power generation. This thesis provides some of the building blocks for enabling this transition.

The first building block concerns the modeling of hydrodynamics and its interactions with the other components that contribute to combustion dynamics. The second is the impact of active control on emissions even while suppressing the pressure instability. The third is the evaluation of model-based active controllers in realistic combustors with configurations that include swirl, large convective delays and unknown changes in the operating conditions. The above three building blocks are investigated in the thesis experimentally in three different configurations. The first is a 2D backward facing step combustor, constructed at MIT, with the goal of investigating the flame-vortex interactions and the impact of active control on emissions. The second is a dump combustor, constructed at University of Maryland, so as to reproduce more realistic ramjet conditions. The third is an industrial swirl-stabilized combustor, constructed at University of Cambridge, to mimic realistic industrial gas combustor configurations which typically include large convective time delays, swirl, and on-line changes in the operating conditions. Results obtained from these three configurations show that through an understanding of the underlying physics and reduced-order modeling, one can design an appropriate actuation,

sensing and control algorithm, all of which lead to model-based active control that reduces pressure oscillations to background noise.

Thesis Supervisor: Anuradha M. Annaswamy
Title: Senior Research Scientist

Thesis Supervisor: Ahmed F. Ghoniem
Title: Professor

Acknowledgments

I would like to first thank Professor Anuradha Annaswamy and Professor Ahmed Ghoniem for their guidance through the five years. Their efforts have been invaluable to open my eyes and carry out my research. I would also like to thank Professor Douglas Hart and Professor Kamal Youcef-Toumi for their support and valuable suggestions during our discussions together.

I owe a great deal to Professor Kenneth Yu and Bin Pang at University of Maryland who gave me the opportunity to investigate their dump combustor in 2003 and 2004.

I am grateful to Professor Ann Dowling and Dr. Alex Riley for giving me a change to implement a Posicast controller in their rig in the summer of 2002.

I would like to thank Adam Wachsman with whom I collaborated for two years, for building the combustor and spending time discussing our research. Also, I owe a great deal to Daehyun Wee for his valuable advices on my research.

I am grateful to Dr. Jean-Pierre Hathout, my predecessor, for his generous help. He was the only person whom I could ask about anything in my first year at MIT.

I would like to thank my colleagues; Ziaieh Sobhani, Debashis Sahoo, Youssef Marzouk, Shanmugan Murugappan, Tongxun Yi, Chengyu Cao, Jaejeen Choi, Murat Altay, Raymond Speth, Daniel Macumber and Mac Schwager for their continued support.

I am very grateful to my parents, Hunkyo Park and Boonle Kim for their love, support and guidance. Finally, a warm and special thanks to my wife, Euene Kwon, for her love and support during the past years.

This work has been sponsored by the National Science Foundation, contract no. ECS 9713415, and in part by the Office of Naval Research, contract no. N00014-99-1-0448.

Table of Contents

List of Figures

1. Introduction

Continuous combustion processes are used in many applications ranging from power generation and heating to propulsion. One of the characteristics of these processes is growing pressure oscillations that transition to a sustained limit cycle. These oscillations occur due to the coupling between acoustics and heat release dynamics. In acoustics, the heat release oscillation supplies volume expansion and this expansion acts as a driving force of the pressure oscillation inside the combustor. This pressure oscillation generates velocity, temperature, and equivalence ratio perturbations, and these perturbations again induce unsteady heat release through heat release dynamics. If this feedback is positive, the combustion system becomes unstable, and the resulting dynamics is referred to as combustion instability [1].

Combustion instability occurs especially in a lean burn condition where the efficiency is high and emission is low [2] or in a rich burn condition where the thermal output is high [3]. The underlying mechanism is complex and changes with the geometry and operation condition making it difficult to develop a single model that describes the dynamics in the whole region. Instead, one needs to divide the operating condition into several sub-categories and develop models that can represent distinct characteristics in those operating conditions [4]. Several investigations have been attempted to develop models at different combustion conditions. At high Damkohler and low Reynolds number condition, a wrinkled thin flame model is used to represent heat release dynamics [5]. In [5], the heat release oscillation is due to the change of the flame area, and the flame area changes by the velocity oscillations. The flame area change by the velocity perturbation is represented using G equation. At other regimes where the Damkohler is

low and the Reynolds number is high, the chemical reaction controls the heat release rate. In this case, a Well Stirred Reactor model has been used to represent the heat release dynamics [6]. In other regions, where hydrodynamics and other mechanisms are important, physics based modeling of the combustion system has not been undertaken rigorously.

To avoid this instability without major modification of the hardware or limitations on the operating conditions, active control has been proposed [7-10]. In active control, pressure or heat flux sensors are utilized to detect the onset of the instability, and actuators such as loudspeakers and fuel injectors, are incorporated to modulate the heat release rate and/or pressure. Early attempts often utilized a phase-delayed form of the pressure sensor signal as an input to a pulsed fuel injector, where the requisite phase delay was determined empirically [7,8]. In the last five to ten years, model-based control has been attempted where it has been shown that an order of magnitude improvement in performance can be obtained over empirical methods [11].

A model-based control strategy is more advantageous since it is based on a quantitative description of the coupling between combustion dynamics and acoustics. This makes the problem amenable to optimization of specific performance goals. Model-based control strategy has been demonstrated successfully over the past several years. Fleifil *et al.* [5] demonstrated that an analytical combustion instability model based on flame kinematics was able to correctly predict experimentally observed unstable modes. Hathout *et al.* [11] designed a linear quadratic regulator based on this model by minimizing a cost function of unsteady pressure and control input, showing that pressure oscillations could be stabilized over a range of frequencies without energizing secondary peaks. Annaswamy *et al.* [12] validated this control design in a 1 *kW* bench-top experimental set up to demonstrate that faster settling time and reduced control effort

could be achieved. Mehta *et al.* [13] extended the flame kinematics model by incorporating the impact of exothermicity and fuel transport. In [6,14,15], it was shown that at high intensities, the heat-release dynamics is modeled more appropriately as a well-stirred reactor. The resulting model was shown to capture drastic changes in the stability characteristics as the operating conditions approached the lean blow-out limit [6]. The same model was shown in [16] to be stabilizable using a self-tuning controller which coped with over a 100% change in the system parameters and retained closed-loop stability.

System identification has also been used to develop dynamic combustion models using input-output data. Brunell [17] used system identification to develop a model and model-based controller for a near full-scale combustion rig under turbulent flow conditions. Murugappan *et al.* [18] developed a system identification model and a LQG-LTR model-based controller for a 30 kW swirl stabilized spray combustor, and succeeded in reducing the overall sound pressure level 14 dB lower than an empirical (non-model-based) phase-shift controller. Neumeier *et al.* [19] developed an observer to estimate the frequencies and amplitudes of the resonant modes which were used to generate control signals. Banaszuk *et al.* [20] used an extremum-seeking algorithm to update the phase angle on-line in the phase shift controller.

Model-based control has also been demonstrated in combustion systems with a large convective time-delay. Hathout *et al.* [21] applied a Posicast (positive forecasting) controller in combustion control for the first time. Evesque *et al.* [22] developed a reduced order adaptive positive cast controller based one a wave-based model formulation and a general heat-release dynamics model

Through these several lab-scale studies, it has been shown conclusively that active control is highly successful in suppressing the pressure oscillations. This success has set the stage for transition of the technology from laboratories to large-scale applications in propulsion and power generation. This thesis provides some of the building blocks for enabling this transition.

The first building block concerns the understanding of the interactions between hydrodynamics and heat release dynamics and their impact on the underlying acoustics in the combustion system. In the cases discussed in the above references, either the flow rates were significantly low [5] or significantly high [6], causing the hydrodynamics to not be significant. Often, however, it has been observed in experiments [23,24] that the hydrodynamic instability does play a dominant role in the acoustic oscillations. A modeling of the interactions between these three mechanisms is therefore crucial in the control of combustors.

The second block is to address the optimization of emissions and other burning characteristics in addition to controlling the instabilities in a combustor. Most of the above mentioned modeling efforts focused on pressure oscillations, neglecting other performance indexes such as emission, efficiency and power density. However, to transform active control strategy from laboratories into commercial applications, it is necessary that this strategy satisfies more than a single performance index. This requires a sensing technology that can detect spatially distributed information describing the response of combustion to the operating conditions and external actuations since conventional pressure signal cannot be used to extract other burning characteristics, e.g., efficiency, signature, emissions and etc. Also, new actuation

methods should be investigated since conventional fuel modulations have the possible emission penalty associated with fuel injection into the combustion zone.

The third is the evaluation of model-based active controllers in realistic combustors with configurations that include swirl, large convective time delays and on-line changes in the operating conditions. In this thesis, I address these building blocks at three different combustor configurations, each of which had its unique characteristics as shown in Table 1-1.

The first is a 2D backward facing step combustor (Configuration I), constructed at MIT, with the goal of investigating the flame-vortex interactions and the impact of active control on emissions. This 2D combustor is an ideal platform to visualize the flame-vortex interactions without requiring any image post processing. The impact of the vortices is bound to make the heat-release quite distributed requiring a sensing technology that can detect spatio-temporal heat release characteristics. For this purpose, a distributed heat release sensor using a 1D photodiode array is used.

For the purpose of simultaneous emission and stability control, air and hydrogen injections are used in Configuration I. While fuel modulation is a common stabilization technique, limitations on this technology include the availability of high bandwidth fuel modulators and the possible emission penalty associated with fuel injection into the combustion zone, where maximum authority is expected. Although control algorithms that accommodate long time delays and hence enable the use of fuel injection upstream of the combustion zone have been formulated [21], there is no guarantee that hot spots would not arise. Instead, air forcing which

occurs very close to the dump plane can deliver high authority for actuation energy. Also, adding additional air at the step tends to decrease the temperature, which is favorable for NO_x reduction. I examine the use of a steady and modulated air jet near the combustion zone and demonstrate its effectiveness as a means for simultaneously suppressing oscillations and reducing NOx, in a case in which the combustion instability is caused by strong flame-vortex interaction. In this regard, an air jet is used to modify the flow structure without implementing major geometric redesign of the flame-anchoring zone [25]. Under some conditions, using an air jet near the lean flammability makes the flame susceptible to blow out. To remedy this situation, I experiment with the addition of small amounts of hydrogen in the primary fuel. It has been shown that adding a small amount of hydrogen to other hydrocarbons can extend the flammability limit and increase resistance to flame extinction [26-31], with potential improvements in the emission trend.

The second is a dump combustor (Configuration II), constructed at University of Maryland, so as to reproduce more realistic ramjet conditions including axisymmetric flow, higher flow velocity and an exit nozzle. In addition, the above-mentioned 1D photodiode array is use to model the flame-vortex interactions and capture the impact of control on spatial combustion characteristics.

Finally, the third is an industrial swirl-stabilized combustor (Configuration III), constructed at University of Cambridge, to mimic realistic industrial gas turbine combustor configurations which typically include large convective time delays, swirl and on-line changes in the operating conditions. Configuration III is a model combustor of a Rolls-Royce RB211-DLE industrial gas

turbine [32]. Control is achieved by modulating the main fuel flow rate in response to a measured pressure signal in the upstream of the combustor. The feedback control is an adaptive controller which can accommodate changes in the resonant frequency and a time lag due to the transport of the fuel [22]. I show from robustness studies that this controller retains control for a 20% change in frequency and a 23% change in air mass flow rate.

In Chapter 2, I discuss simultaneous control using new actuation strategy in Configuration I. In Chapter 3, a new sensing technology capturing spatio-temporal heat release characteristics will be discussed in Configuration II. In Chapter 4, validation of the active control strategy in Configuration III will be shown.

Table 1-1 Configurations of the three combustors considered

	Configuration I	Configuration II	Configuration III
Location	MIT	U. Maryland	U. Cambridge
Power	50-80kW	50kW-300kW	80-250kW
Geometry	2D Step	Axisymmetric Dump	Swirl stabilized
Application	Simplified gas turbine Ramjet engine	Ramjet engine	Industrial gas turbine
Reynolds number	6000-8000	25000-150000	100000
Upstream mean velocity	5m/s	15-100m/s	26m/s
Fuel Type	Propane (main fuel) Hydrogen(modulation)	Ethylene (main fuel) Ethanol(modulation)	Ethylene (Main fuel modulation)
Feedback Sensors	Pressure	Linear photodiode array	Pressure
Controllers	Static on-off Phase shift Adaptive Posi-cast	Adaptive Posicast	Adaptive Posicast Phase shift
Actuators	On-off valve (Air jet) Proportional (H_2)	On-off valve	Proportional valve
Actuation Location	Step	Dump plane	Upstream of the swirler
Collaborators	A.Wachsman Z. Sobhani	Dr. K. Yu B. Pang	Dr. A. P. Dowling Dr. S. Evesque Dr. A. Riley

2. Simultaneous Stability and Emissions Control

(Configuration I: MIT Backward facing Step Combustor)

In this Chapter, I experiment air forcing as an actuator for the purpose of simultaneous stability and emissions control. While fuel modulation is a common stabilization technique, limitations on this technology include the availability of high bandwidth fuel modulators and the possible emission penalty associated with fuel injection into the combustion zone, where maximum authority is expected. Air forcing which occurs very close to the dump plane can deliver high authority for actuation energy. Also, adding additional air at the step tends to decrease the temperature, which is favorable for NO_x reduction. Under some conditions, using an air jet near the lean flammability makes the flame susceptible to blow out. To remedy this situation, I experiment with the addition of small amounts of hydrogen in the primary fuel. I show that, with air injection and a small amount of hydrogen addition, one can simultaneously reduce pressure oscillations up to 15 *dB* and reduce NOx emission to sub-*ppm* levels. Section 2.1 describes the combustor setup. Section 2.2 discusses the combustion dynamics. Finally, simultaneous control results are in Section 2.3.

2.1 Experimental Setup

The experimental test-bed is a backward-facing step combustor which provides a sudden expansion with recirculation zone that anchors the flame, as shown in Figure 2-1 and Figure 2-2. It consists of a rectangular stainless steel duct with a cross sectional area 40 *mm* high and 160 mm wide. Halfway along the length of the combustor, a ramp contracts the channel height from 40 *mm* to 20 *mm*, followed by a constant-area section and a sudden expansion back to 40 *mm*. The step height is 20 *mm*. The overall length of the combustor is 1.9 *m*, with the step located in the middle. The air inlet to the combustor is choked. The exhaust gases are expanded at the end of the chamber. The combustor is equipped with quartz viewing windows. An air compressor supplies air up to 110 *g/s* at 883 *kPa*. Propane is used as the primary fuel. Fuel is supplied at several spanwise holes from a fuel manifold located upstream of the step, at 17.5 *cm* or 35 *cm*. Fuel is injected in the opposite direction to the flow to improve mixing. The sensors and actuators are positioned as indicated in the figure. In the figure, p' is pressure fluctuations, $\overline{U}$ is the mean air velocity in the upstream, u_1' and u_2' are velocity fluctuations at the point of fuel injection and the step, respectively, Q' is the fluctuation in the heat release rate in the burning zone, ω' is vorticity fluctuations in the downstream from the step and A_{fuel} and A_{air} are fuel and air forcing for control.

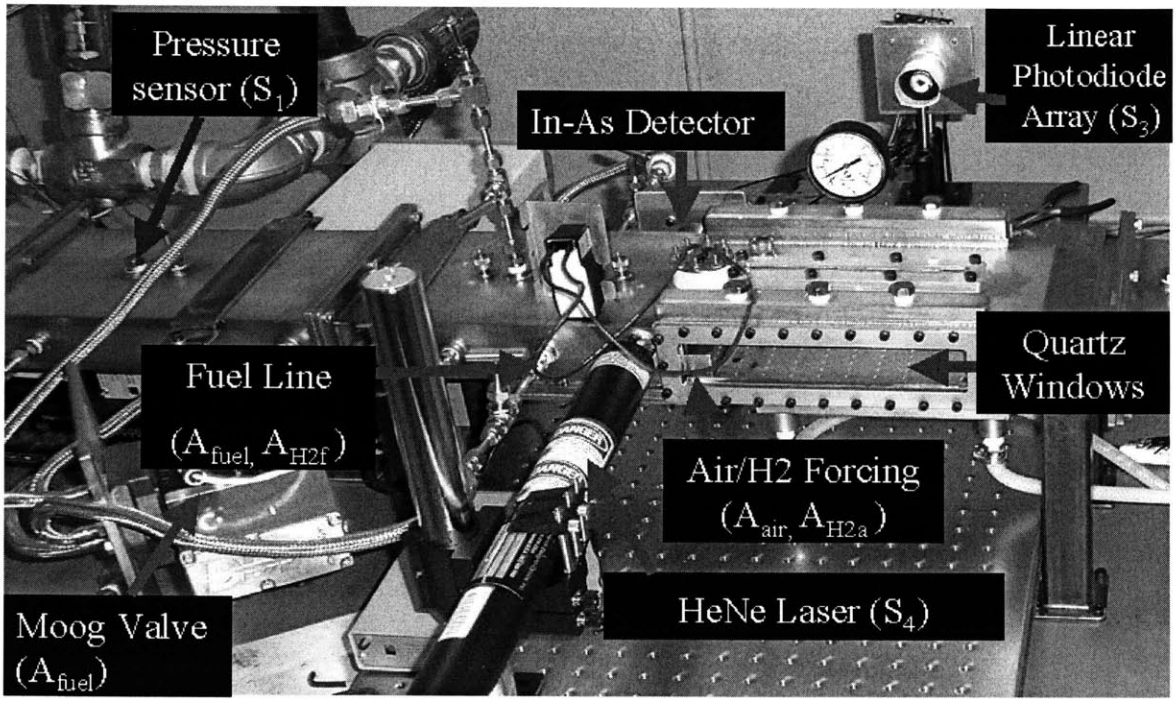

Figure 2-1 Photograph of the MIT backward facing step combustor with various sensors and actuators

Here, I describe the sensors used in the backward facing step combustor. Pressure fluctuation is measured with the Kistler pressure sensors (S_1). CH* chemiluminescence, which can be related to heat release fluctuation is measured with the linear photodiode array (S_2). 2D flame structure is measured with a high-speed camera (S_3). Equivalence ratio fluctuation is measured with the laser and photodetector arrangement (S_4). The pressure and equivalence ratio measurements are logged at 1000 *Hz* by a Pentium III with a dSPACE data acquisition board installed. The linear photodiode array voltages are captured by a Pentium IV with National Instruments data acquisition hardware installed. The overall sample rate is 64 kHz to read all the photodiodes, and each snapshot is captured at 500 Hz. In the following, detailed descriptions of the sensors are provided.

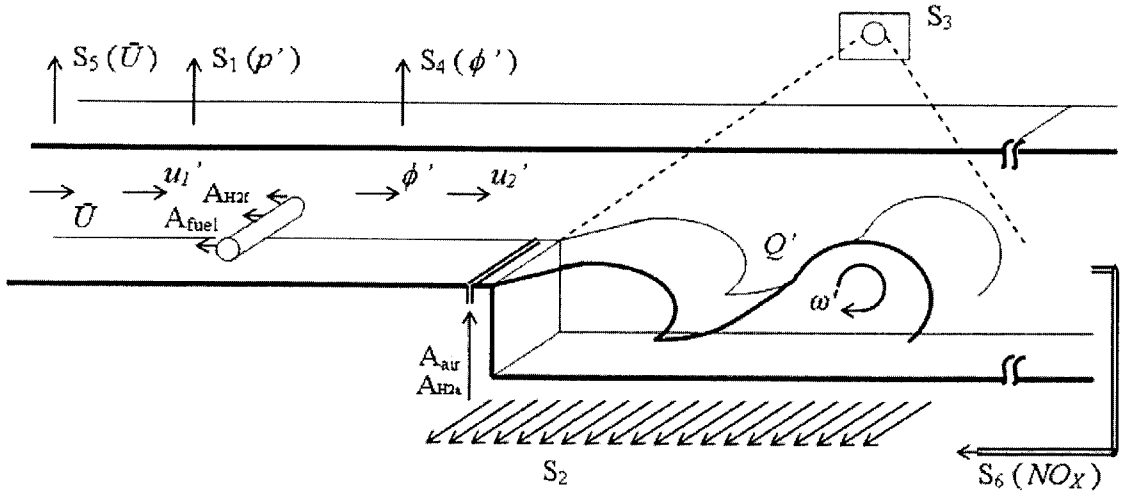

Sensors		Variables	
S_1	Pressure Sensor (p')	p'	Pressure Fluctuations
S_2	Linear Photodiode 128-array (Q')	Q'	Heat Release Fluctuations
S_3	High Speed Camera	ω'	Vorticity
S_4	Equivalence Ratio Sensor (ϕ')	ϕ'	Equivalence Ratio Fluctuations
S_5	Air Flow Meter ($\bar{U}$)	$\bar{U}$	Mean Air Flow Rate
S_6	Emissions (NO_X)	u_1'	Velocity Perturbations at the step
Actuators			
A_{air}	Air Forcing	u_2'	Velocity Perturbations at the fuel bar
A_{fuel}	Fuel Forcing		
A_{H2f}	H2 Forcing with the Fuel		
A_{H2a}	H2 Forcing with Air		

Figure 2-2 Schematic of the backward facing step combustor with various sensors and actuators

2.1.1 Sensors

Pressure Sensors (S_1)

Kistler pressure sensors are used to measure the dynamic pressure response from the interior of the combustor. The 6061B ThermoCOMP Quartz Pressure Sensor can measure 0-2.5 *bar* up to 0-250 *bar*. It is water-cooled and designed especially for small combustion engines and for thermodynamic investigations in the laboratory.

Linear Photodiode Array (S2)

CH* chemiluminescence is measured spatially and temporally using a new sensor design involving a linear photodiode array to capture distributed heat release characteristics [33,34]. An NMOS linear image sensor (S3901-128Q) is available from Hamamatsu Photonics that provides 128 individual photodiodes in a linear array. Each pixel is 2.5 *mm* high and 45 μm wide. A flame image can be projected onto this array using the appropriate optics, and a "linear snapshot" can be taken. This has an advantage over a single photodiode, because it provides spatial information. It also has an advantage over a CCD camera, because the data can more easily be streamed to a computer for analysis, and the amount of data can be handled in real-time for control purposes. Each pixel integrates the light intensity over time, and resets when it is read.

In the experiment, the flame image passes through an optical bandpass filter centered at 430 *nm*, the wavelength of CH* chemiluminescence (Figure 2-3). Unlike most CCD arrays which have peak sensitivity in the infrared region, the linear photodiode array has a high UV

sensitivity, making it suitable for this application. A bi-convex UV fused silica lens is used to focus the image of the flame onto the chip. The photodiode array has high spatial resolution in the streamwise direction, and integrates the light intensity in the vertical direction.

High Speed Camera (S_3)

To capture 2D flame images at a high resolution and high speed, a MotionPro CMOS camera from Redlake is used. The MotionPro system is designed to capture high-speed digital images and deliver them directly into a PC for analysis and documentation with maximum frame resolution of 1280 x 1024 pixels with record rates up to 1000 frames per second. Flexible recording options permit using the PCI-board memory as a circular buffer into which specified pre- and post-trigger frames are recorded, or dividing it into a segmented buffer for multiple session operation.

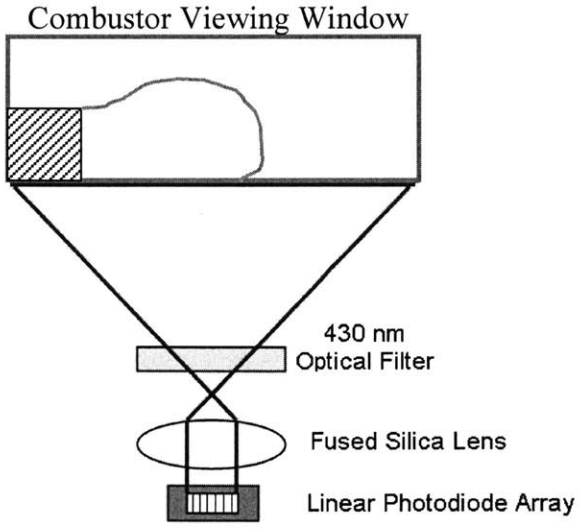

Figure 2-3 Linear Photodiode Array Sensor (S_2) Schematic. The flame image is filtered for CH* chemiluminescence and focused onto the linear photodiode array.

Equivalence Ratio Sensor (S_4)

The equivalence ratio sensor uses a laser and a photodetector. The laser emits a beam of light of the wavelength (3.39 μm) that is absorbed by hydrocarbons like methane and propane [35]. On the other side of the combustor, a detector is installed that is sensitive to that wavelength of light. When fuel passes through the laser beam, it absorbs some of the laser light and the detector signal is reduced. The intensity of the light can be related to fuel concentration using the Beer-Lambert law, as described by Lee *et al.* [35].

$$I / I_o = 10^{-\int_0^l \varepsilon c dx},$$

where I_o is the intensity of incident monochromatic light, I is the intensity of transmitted light through the absorbing species, ε is the decadic molar absorption coefficient (cm^2/mol), l is the absorption path length, and c is the concentration of absorbing species (mol/cm^3). Figure 2-4 shows the schematic of the device as installed in the step combustor.

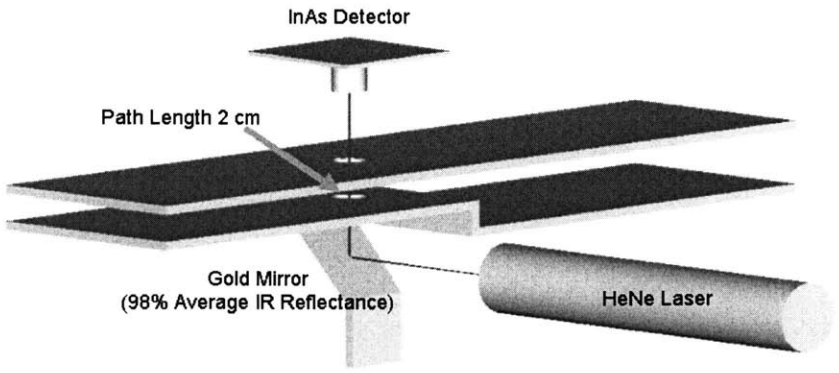

Figure 2-4 Equivalence Ratio Sensor (S_4) Setup

Air Flow Sensors (S_5)

The air mass flow meter is a Sierra Instruments 780S-NAA-N5-EN2-P2-V3-DD-0 Flat-Trak. The maximum flow rate is 173 *g/s*. The maximum pressure is 827 *kPa*. The unit is powered by an 18-30 V DC power supply, and it outputs a signal from 0-10 V DC which is proportional to the mass flow rate of the air.

Emission Sensors (S_6)

Emissions sensors are installed on the rig to provide quantitative measurements of performance characteristics such as NO_x concentration and burning efficiency. Fuel modulation is a common stabilization technique. The impact of fuel fluctuations on emissions and efficiency has been measured, but the results have not been used in the feedback loop in a way that optimizes several performance parameters simultaneously at a fixed operating condition [36,37]. Additionally, a study of emissions will provide insight into the possibility that air forcing produces cleaner emissions and more complete burning than fuel modulation. For example, air injection at the step may serve to cool the flame, reducing NO_x.

Other uses for this equipment will be to correlate the linear photodiode array with emissions characteristics. For example, it appears that the flame becomes more compact when controlled with air injection. Compact flames are associated with low emissions because of decreased residence time in which to form NO_x. Preliminary analysis of linear sensor images appears to show this compact flame shape after control is applied. If a correlation can be made between emissions and linear sensor image, it is possible that the linear sensor could serve as an inexpensive surrogate for an emissions sensor.

An NO_x emissions sensor has been installed in the combustor rig. The emissions probe is located 62 *cm* downstream from the step in the exhaust section. The probe extends 20 *mm* (half the combustion chamber height) into the chamber, through a ½-NPT threaded boss. The probe is attached to a Universal Analyzers Model 270S Stainless Steel Heated Stack Filter. The sample line is connected to a Universal Analyzers Model 520 Single Channel Sample Cooler. The cooler brings the sample down to 4 °C. A peristaltic pump removes to the exhaust trench the water that is condensed by this operation. The cooled sample is sent to the Thermo Environmental Instruments Model 42C High Level NO-NO_2-NO_X Analyzer.

2.1.2 Actuators

In the following, I describe the air and fuel actuators. As indicated in Figure 2-2, the fuel injection occurs several step heights upstream pointing upstream for uniform spanwise mixing. Fuel can be modulated at the fundamental unstable frequency, but since the fuel has time to mix in the streamwise direction before it reaches the flame, the authority of fuel modulation is reduced. Also, this type of actuation introduces a delay between the time the fuel is modulated and the time the fuel encounters the flame, which is not only moving, but also spatially distributed. Air forcing which occurs very close to the dump plane can deliver high authority for actuation energy. Also, adding additional air at the step tends to decrease the temperature, which is favorable for NO_x reduction. Detailed description of the air and fuel actuation is in the following and closed-loop control results with air actuation will be shown in Section 2.3.

Forcing Air (A_{air})

Control actuation is accomplished using Dynamco D1B2204 Dash 1 direct solenoid poppet air valves. This valve can supply 1.8 *g/s* of air when supplied with 689 *kPa*. The valve is connected to a plenum beneath a 2 *mm* spanwise slot and 12 *mm* upstream of the step.

Fuel Forcing (A_{fuel})

Another valve used for actuation is the Moog D633-7315 AIC Direct Drive Valve (DDV). It has its own built in feedback loop to ensure the spool position using an LVDT. This feedback loop is controlled by the Moog D143-098-013 Single Axis Electronic Controller. This unit is powered by a 48V Condor Power Supply, which also powers the valve. The controller accepts inputs from -10 VDC to 10 VDC.

A transfer function for this valve was determined using system identification. White noise with a bandwidth of 1000 *Hz* was the input. The spool position, measured with the LVDT was the output. The spool position is related to mass flow rate by a calibration. The transfer function is

$$G_c(s) = \frac{\dot{m}(s)}{V(s)} = \frac{0.03837s^3 - 69.11s^2 + 1.786\times10^5 s + 1.495\times10^8}{s^4 + 2634s^3 + 7.934\times10^6 s^2 + 1.034\times10^{10} s + 3.946\times10^{12}}$$

where $\dot{m}$ is mass flow rate (*kg*/s) and V is the input to the valve (Volt). The Bode plot in Figure 2-5 indicates resonance at 378 *Hz*.

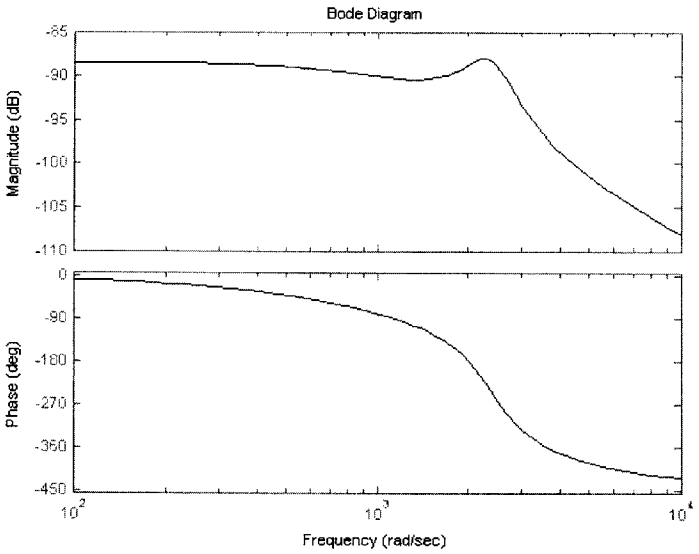

Figure 2-5 Moog DDV Bode Plot (Bandwidth is 444*Hz*)

H2 (A_{H2f} & A_{H2a}) Injection

To extend the flammability limit and increase the resistance of the flame to extinction, hydrogen is delivered at 0-9 *mg/s* through a Sierra Instrument mass flow controller. Hydrogen is either mixed with propane and introduced through the fuel bar, A_{H2f}, or mixed with the air jet and introduced through the slot, A_{H2a}.

2.2 Modeling of Combustion Dynamics

Figure 2-6 shows schematically how various flow, combustion and acoustics mechanisms interact, and their contributions to the combustion dynamics and emissions. This model features the following:

- The feedback mechanism that contributes to combustion dynamics, which couples heat-release dynamics and acoustics.
- The heat-release perturbations that arise due to fluctuations in the equivalence ratio, ϕ', and hydrodynamic perturbations, ω'.

Optimal actuation for control depends on the mechanism leading to combustion instability. For example, if equivalence ratio fluctuations play a significant role, upstream fuel modulation may work best. On the other hand, if flame-vortex interaction is the governing mechanism, hydrodynamic-based actuation near the step, such as spanwise air injection, would be more effective. A parametric study of the impact of the inlet conditions and the hydrodynamics on the combustion instability is shown in the following sections.

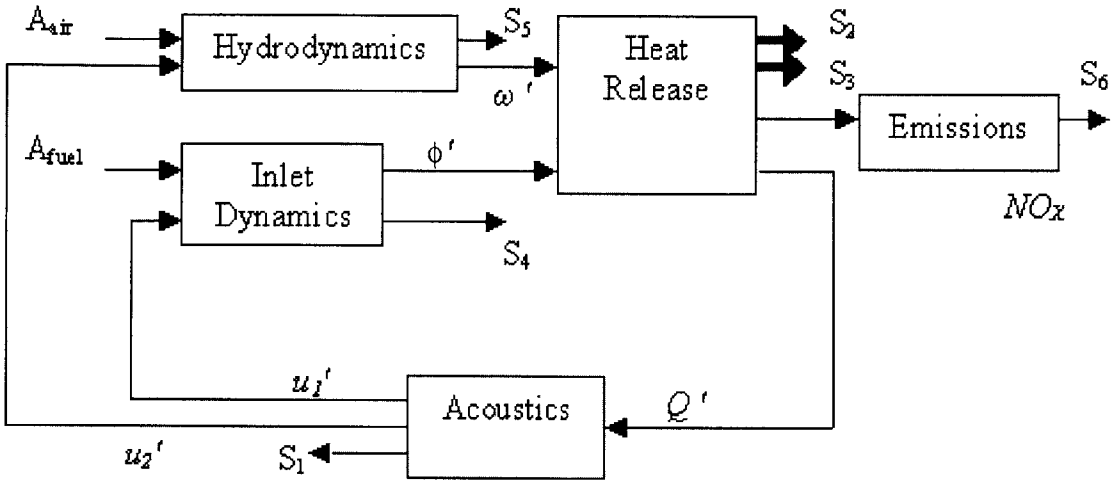

Figure 2-6 Schematic diagram of the acoustics, hydrodynamics and heat release dynamics and their interactions.

2.2.1 The Role of the Inlet Dynamics (Mixture Inhomogeneity)

I first examine the role of fuel/air mixture inhomogeneity, ϕ', in the combustion dynamics. Equivalence ratio fluctuation occurs due to velocity perturbations, u_1', at the point of fuel injection according to $\phi' = \overline{\phi} \dfrac{1}{1 + \dfrac{u_1'}{\overline{U}}}$ (if $u_1'/\overline{U} < 1$). ϕ' appears at the burning zone following a convective transport time delay, τ_{tot}, determined by the mean mixture velocity, $\overline{U}$, and the distance from the point of fuel injection to the burning zone, L, $\tau_{tot} = \dfrac{L}{\overline{U}}$ [21,38]. Fluctuations in fuel/air mixture produce heat release fluctuations, Q', proportional to ϕ'.

The convective delay from the point of fuel injection to the burning zone determines the phase between ϕ' and u_1' (and hence p'). The time delay can be modified by changing the fuel injection location. To determine the impact of the mixture inhomogeneity, or ϕ' on stability, the location of the fuel bar was varied and the pressure was measured at various air and fuel flow rates. Moving the fuel injection further upstream has the following effects: 1) the convective time delay is increased, and 2) the amplitude of mixture inhomogeneity is decreased due to diffusion and reduction in u_1' (the fundamental acoustic mode in the combustor is a quarter-wave mode with a closed end upstream and an open end downstream). Note that the hydrodynamic characteristics do not change by changing the fuel injection location.

I now consider two cases: I and II, where the fuel bar was located 17.5 *cm* and 35 *cm* upstream from the step, respectively. In both cases, the uncontrolled combustor was operated at different air-flow rates. Figure 2-7 shows the effect of varying the equivalence ratio and Reynolds number on the overall sound pressure level (OASPL). In all these experiments, the excited acoustic mode frequency, f_{ac}, was 38 *Hz*. In Figure 2-7(b), the pressure level almost monotonically increases with the Reynolds number while it is insensitive to the changes in the mean equivalence ratio. In contrast, in Figure 2-7(a), the impact of Reynolds number is non-monotonic showing reduced pressure level at Re = 8500 and increasing suddenly at Re = 9500. Also at Re = 9500, the pressure level is sensitive to the changes of the mean equivalence ratio. Similar observations (pressure level increases with the increase in the Reynolds number and is sensitive to the mean equivalence ratio change at high Reynolds number) have been made in Ref. [39] in a bluff body stabilized dump combustor.

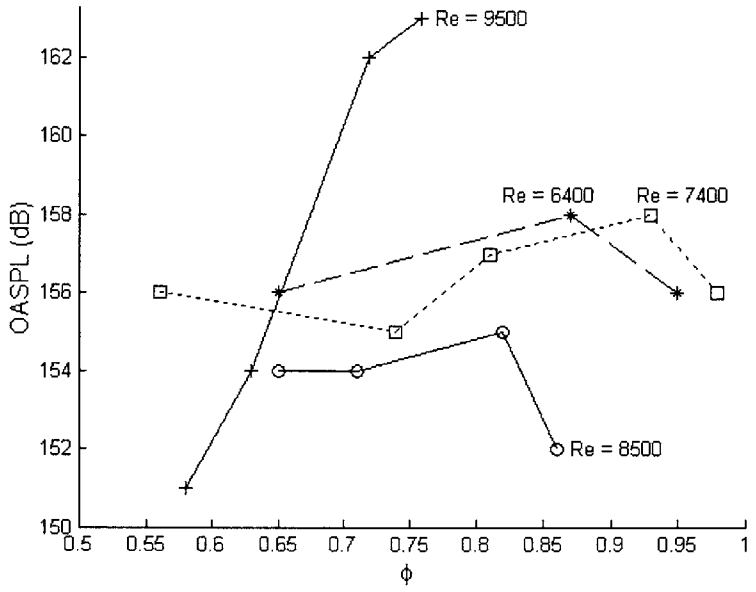

(a) Case I (fuel bar at 17.5 *cm*)

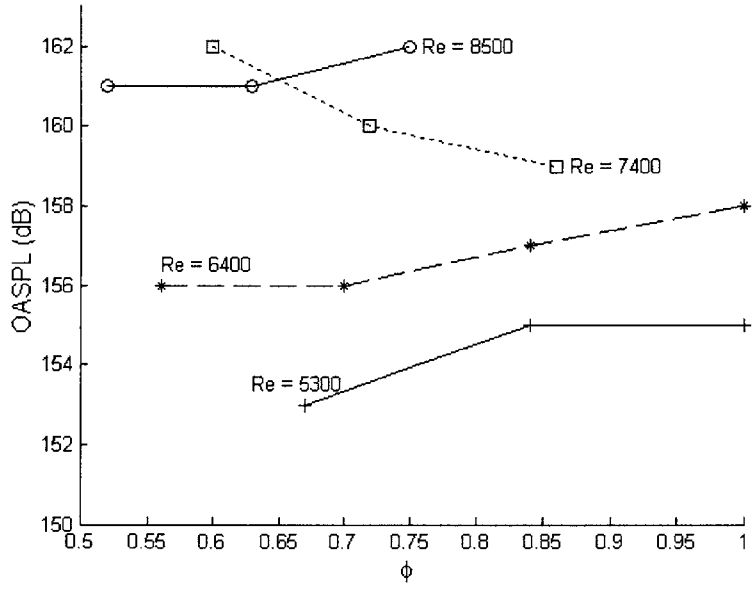

(b) Case II (fuel bar at 35 *cm*)

Figure 2-7 The impact of varying equivalence ratio and Reynolds number on the overall sound pressure level in Cases I and II.

To understand this discrepancy in Cases I and II, this stability map is redrawn with the convective time delay, τ_{tot}, as the x axis as shown in Figure 2-8. The convective time delay from

the fuel injection point to the step is shown in the figure as multiples of τ, where τ is the acoustic time scale, $1/f_{ac}$ = 26.3 *ms*. If the instability was controlled by the mixture inhomogeneity only, a stability band should appear in these maps as the time delay is varied as follows: stable zones when the transport delay is between $n\tau$ and $(n+0.5)\tau$ and unstable zones when the delay is between $(n+0.5)\tau$ and $(n+1)\tau$ [21,38]. No changes in the pressure fluctuations were shown in Figure 2-8(b) during these transitions indicating that mixture inhomogeneity does not play a role in Case II. However, in Case I, a pressure drop is observed when the time delay is between τ and $(n+0.5)\tau$ indicating that the equivalence ratio oscillation has a secondary role. This secondary role of the equivalence ratio oscillations in Case I explains the non-monotonic relation between the pressure level and the Reynolds number observed in Fig. Figure 2-7(a).

I further investigated the extent to which the mixture inhomogeneity contributes to combustion instability. Equivalence ratio oscillations (S_4) and the corresponding pressure signal (S_1) are compared in Cases I and II at two different operating conditions. First, at Re = 5300 and ϕ = 0.85, as shown in Figure 2-9(a), negligible equivalence ratio fluctuations are observed in Case II due to streamwise diffusion, while significant equivalence ratio fluctuations are observed in Case I. The pressure amplitude is higher in Case I indicating that the equivalence ratio fluctuation increases the pressure oscillations at this operating condition. Note that Case I is in the band between $(n+0.5)\tau$ and $(n+1)\tau$. On the other hand, even without equivalence ratio fluctuations, pressure oscillations are still significant in Case II.

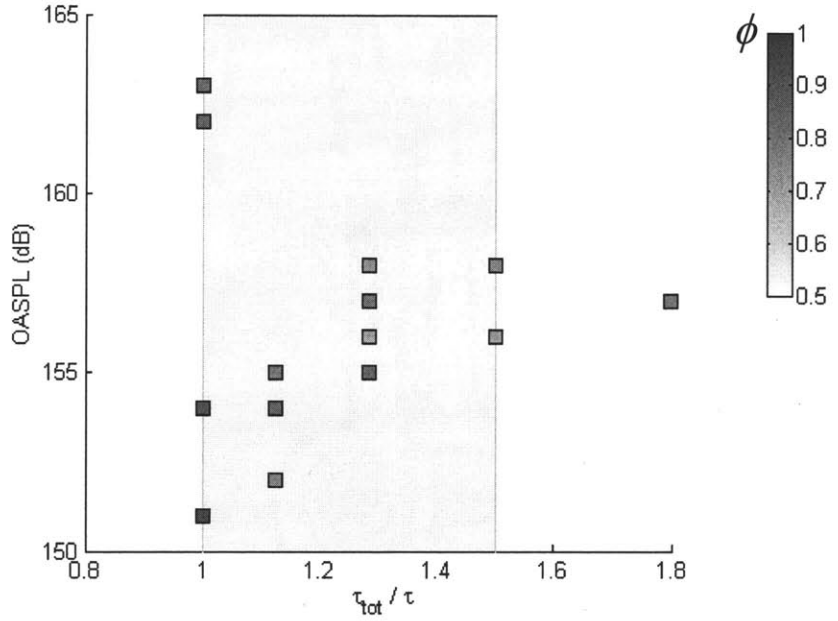

(a) Case I (fuel bar at 17.5 *cm*)

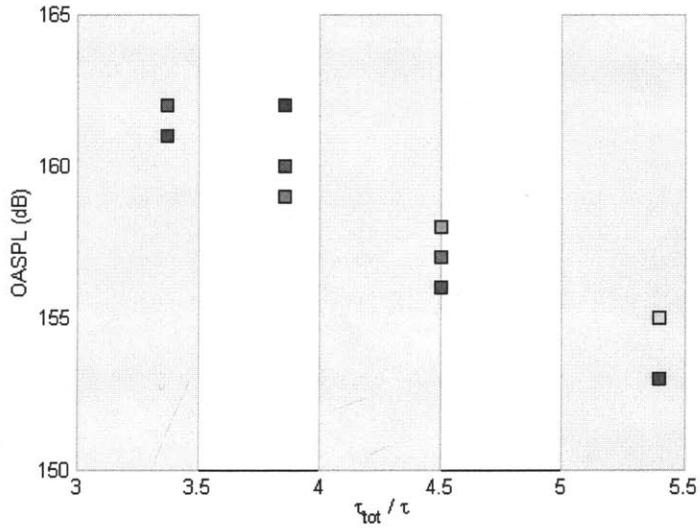

(b) Case II (fuel bar at 35 *cm*)

Figure 2-8 The impact of convective time delay on the overall sound pressure level in Cases I and II.

The power spectra obtained at a second operating condition, at Re = 8500 and ϕ = 0.65, are shown in Figure 2-9(b). This condition corresponds to a band between $n\tau$ and $(n+0.5)\tau$ in

both cases, where equivalence ratio oscillations may damp out pressure oscillations. While significant equivalence ratio fluctuations are present, Case II has lower values since the fuel bar is positioned further upstream, similar to the Re=5300 experiment. Since the equivalence ratio fluctuations, under these conditions, provide negative feedback, Case I exhibits a lower pressure amplitude. However, both cases show significant pressure oscillations, indicating that the essential mechanism here is not mixture inhomogeneity.

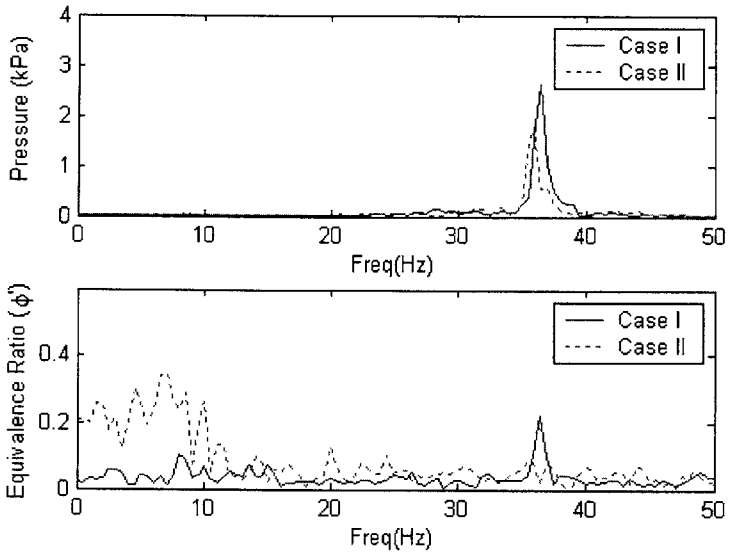

(a) Re=5300, ϕ=0.85

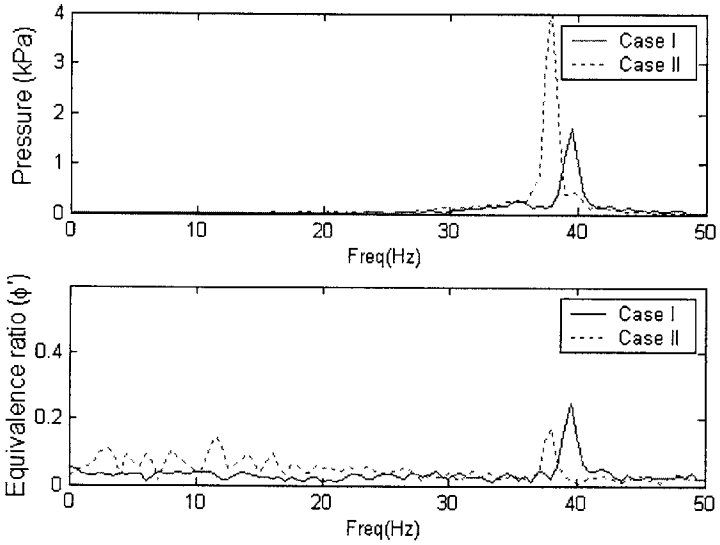

(b) Re=8500, ϕ=0.65

Figure 2-9 Pressure (S_1) and equivalence ratio (S_4) frequency spectra at (a) Re=5300 and ϕ=0.85 and (b) Re=8500, ϕ=0.65 in Cases I and II.

2.2.2 The Role of Hydrodynamics and Flame-Vortex Interactions

Velocity perturbations can cause repeated shedding of vortical structures at the step. This, in turn, causes the flame shape to change, thereby generating large amplitude of heat release fluctuation. This vortex shedding has a preferred frequency quantified by a Strouhal number $St = f_H H / \overline{U} = O(0.1)$ where H is the step height and f_H is the frequency in Hz [40]. If the preferred vortex shedding frequency is near the acoustic mode frequency, f_{ac}, the system is more prone to combustion instability.

The strong dependency of combustion instability on the Reynolds number or the mean velocity described above suggests that the primary mechanism causing combustion instability is the hydrodynamics and its interaction with flame. As mentioned before, hydrodynamics has a preferred frequency around $f_H = O(0.1\overline{U} / H)$. Interestingly, strong instability occurs above Re=9500 in Case I, and Re=7400 in Case II, as shown in Figure 2-7, in which the preferred frequency is f_H =33Hz and 25Hz, respectively, both of which are close to the acoustic frequency, f_{ac}=38Hz. High speed CCD images in Figure 2-10, captured at 500 *frames/s,* show strong flame–vortex interactions with no noticeable difference in the flame structure between the two cases. These images confirm the role of flame-vortex interactions in the combustion instability mechanism.

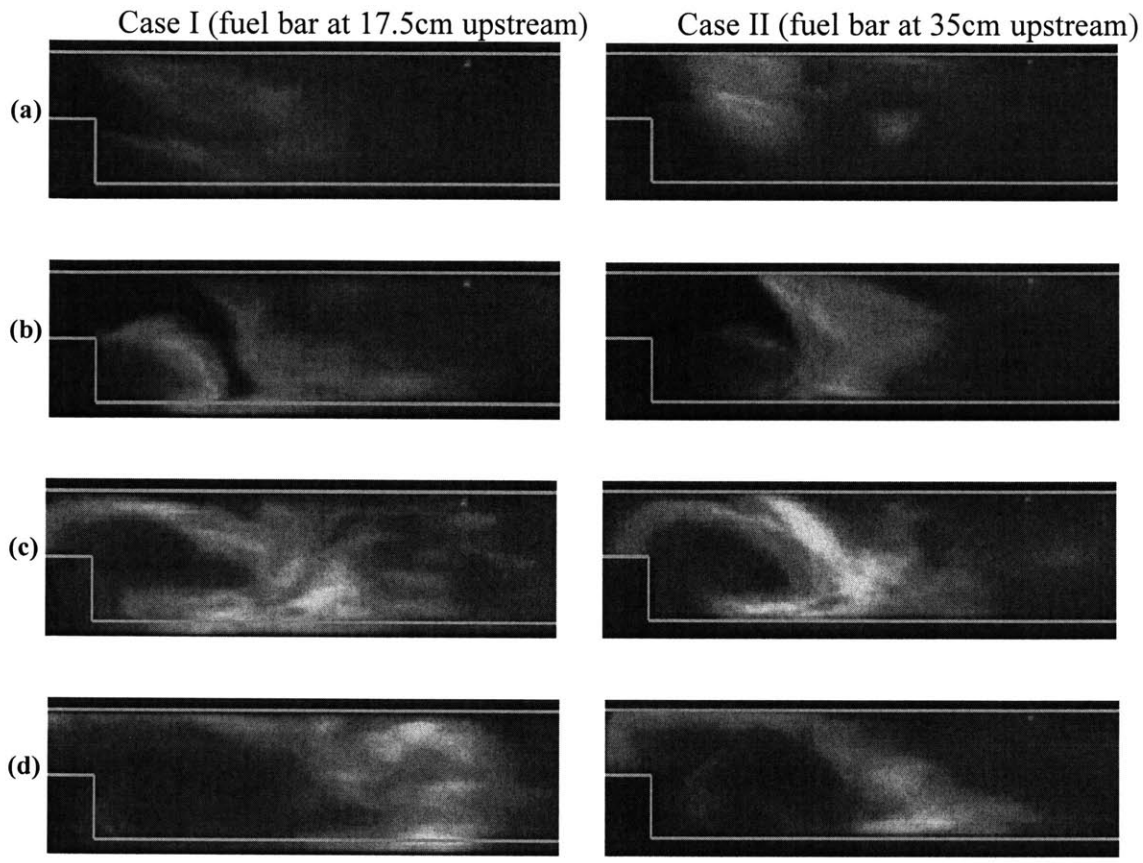

Figure 2-10 High speed CCD images of the flame in the backward-facing step combustor at Re=6300 and ϕ=0.85, in Cases I and II at different moments in the cycle. (a) p'=0 and dropping, (b) minimum p', (c) p'=0 and rising, and (d) maximum p'.

Now, I now show the cyclical flame-vortex interactions using high-speed imaging. We start the analysis of the mechanism from the moment of maximum velocity, according to Figure 2-12 (numbers between brackets correspond to the image number in the figure). Figure 2-11 shows 8 snapshots of the flame from the video record, successive images are separated by 4 *ms*, that is, the cycles ends almost halfway between (7) and (8) since the cycle time is close to 25 *ms*. Around the moment of maximum velocity, the flame appears as a vertical front moving downstream of the step (1). Note that due to a combination of local small-scale turbulence and relatively weak variation in the spanwise direction, the flames appear as thick zones. As the velocity decreases gradually, the flame advances into the channel, forming two fronts, a leading

vertical front that accelerates forward on the top half of the channel, and a horizontal front that extends back to the step (2). It is interesting to observe near-extinction at the step during this part of the cycle, apparently due to the high flow velocity/strain rates there (2-3). As the velocity becomes negative, the vertical flame curves slightly forward as it moves faster along the upper wall than the lower wall, and the horizontal flame curves upwards, away from the step, and forms a forward fold closer to the lower walls (4). As the flame departs from the step, it burns vigorously into the inlet channel (4-5). Meanwhile, reactants are trapped in the fold, and in between the fold and the leading curved flame (5). The inception of the fold can be seen in (3-4) clearly, as well as the formation of reactants traps between the fold and the leading vertical flame (4-5). During this part of the cycle, the curved horizontal flame propagates almost vertically towards the top wall, pushing its leading and trailing edges downstream and upstream, respectively, with the latter migrating further into the inlet channel (4-6). As the velocity emerges from the negative region, the flames surrounding the fold start to converge inward, burning the trapped reactants and closing the gaps (5-6). According to the images, this is the moment of maximum total burning rate. Meanwhile the migration of the trailing edge of the flame into the inlet channel, which started when the velocity delved into the negative domain, is halted as the velocity recovers (5-7). Signs that the flame was pushed back towards the step while the velocity was rising towards its maximum are seen in (7). The cycle is now over, and (8) is well into the new cycle.

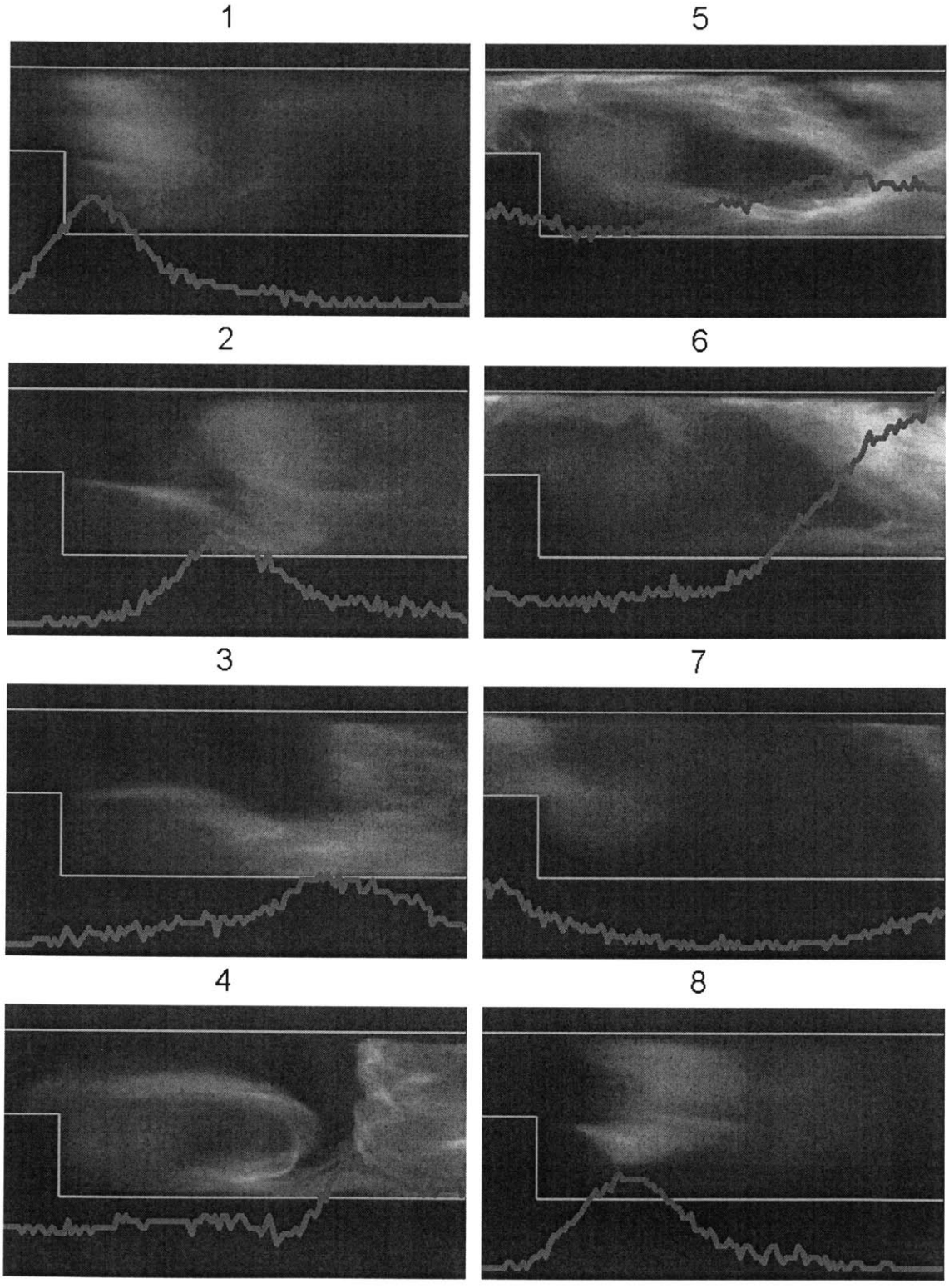

Figure 2-11 High speed CCD images, and the CH* data captured by the linear photodiode, images were captured at 500 *Hz*, and represent slightly more that one cycle.

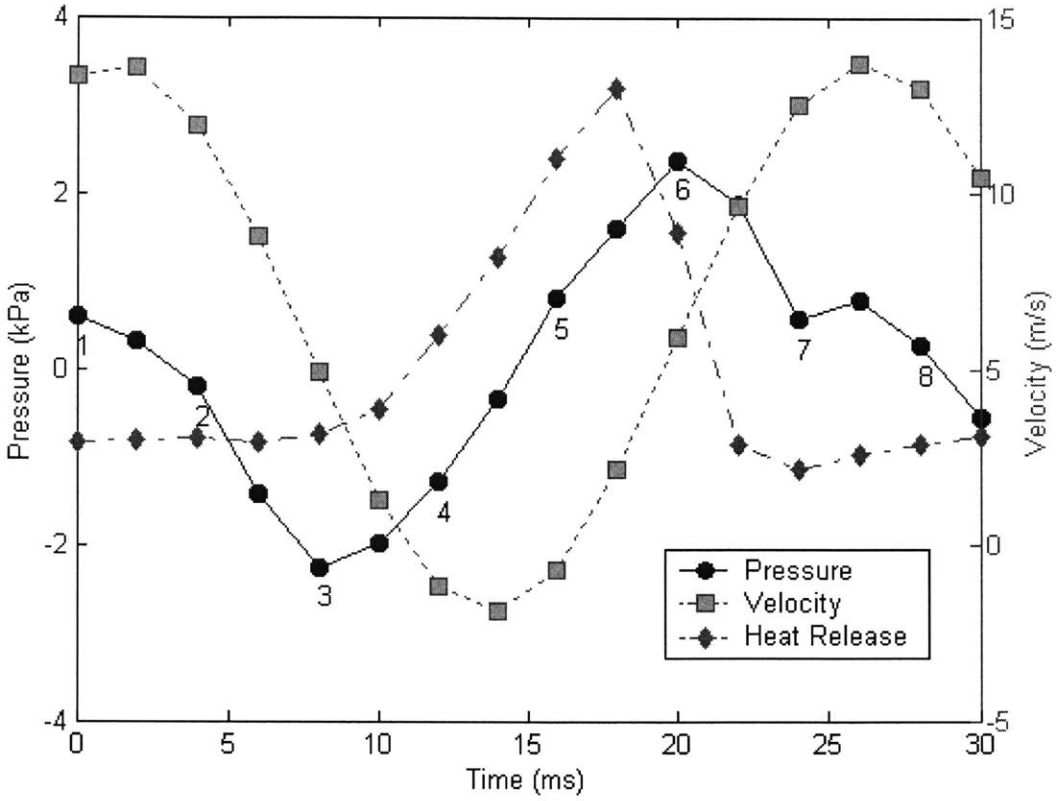

Figure 2-12 Pressure, velocity and heat release rate, with the numbering of the points corresponding to frames in Figure 2-11.

Now, we look closely at the CH* data to correlate the flame geometry, the heat release rate and the pressure. At the beginning of the cycle, the CH* distribution peaks near the step, where the flame front is located at that moment (1). As the flame propagates downstream, the CH* distribution advances with it (2), stretching downstream with a flatter peak as the two parts of the flame become distinguishable (3). Consistent with the video images that shows partial extinction at the step, CH* signal there is near zero (2-3), until the flame is pushed away from the step and into the inlet channel (4). We note the strong correlation between the brightness of the video image and the local CH* signal, confirming the intended use of the former as a surrogate for burning intensity. As the horizontal flame curves upward and away from the high strain zone,

near the step, a weak CH* signal starts to appear there, growing slowly in a nearly flat distribution behind the leading peak (4-6), the latter corresponding to a more energetically burning and folding flame that continues its forward propagation (5). One can clearly see the sign of a flame advancing upstream in the CH* image in (5). As the flames converge towards the centers of the folds, the leading peak in CH* rises significantly, heralding the peak heat release rate (6). This is followed by a rapid drop in CH* throughout the channel, except in the inlet channel where a flame is convected back downstream, following its brief early migration there (7). The flame moving downstream the step is again captured in the CH* in (7-8).

The streamwise integral of CH* represents the instantaneous total heat release rate, shown in Figure 2-12. The fast but more gradual rise in total heat release, followed by the faster drop and slow recovery are clearly depicted in this figure. Because of the dynamics described in the previous paragraphs, the total heat release rate peaks almost 100^{o} ahead of the velocity at the step, at a moment when the velocity near the step is still relatively low but rising. As can be seen in the same figure, and because the dominant acoustic mode is a quarter wave mode, the pressure also leads the velocity by 90^{o}, and the pressure and heat release rate are in phase, as expected in an unstable combustor. The mechanism responsible for this coupling is clearly fluid dynamic in nature, and is embedded in how the flow downstream the step causes the flame convolutions shown in Figure 2-11. Next, we examine the Schlieren images to confirm the close relationship between the bright zones in the direct video images and the burning zones, or "thick" flames in the case we analyze here.

Figure 2-13 shows the Schlieren images taken from another cycle but corresponding to the same case shown in Figure 2-11, with the CH* concentration superimposed on the images as

before. Statistical variations are responsible for the small differences between the images shown in Figure 2-11 and Figure 2-13, however the similarity is nevertheless very strong. In general, the Schlieren images are better indicators of the flame front surface than the direct video since they capture the density gradient. However they can be affected more by the spanwise averaging, and by heating due to the proximity of walls, e.g., close to the step, which can introduce weak local density gradients in the absence of flames. Despite that, the Schlieren images show strong resemblance to the direct video images, and are also strongly correlated with the CH* distributions.

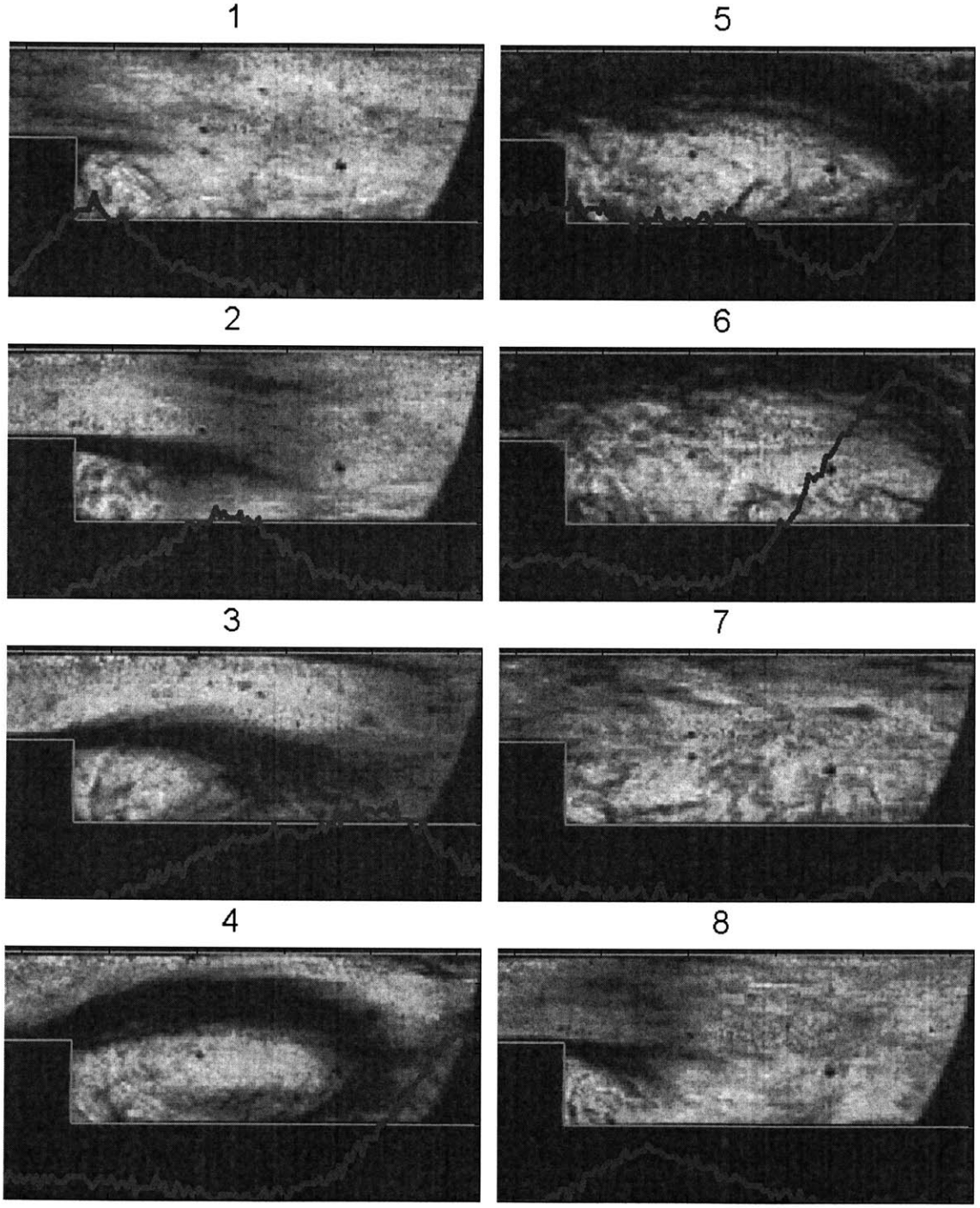

Figure 2-13 Schlieren images with CH* data.

2.3 Simultaneous Control of Combustion Instability and Emissions

In this section, I show open and closed-loop control results using the air jet and H2 addition, in order to simultaneously reduce pressure oscillations and NOx emissions. The fuel bar is located 35 *cm* upstream of the step. In Section 2.3.1, I consider a static air jet (A_{air}) near the step and H2 addition to the primary fuel (A_{H2f}). In Section 2.3.2, I show the impact of modulating the air jet (A_{air}) when it is mixed with hydrogen (A_{H2a}). Primary fuel modulations (A_{fuel}) at the fuel bar were also attempted, but, as expected from the results of Section 2.2, its impact on combustion instability was negligible.

2.3.1 Static Air (A_{air}) and H2 injection (A_{H2f})

The effect of a steady transverse air jet (A_{air}), introduced a short distance upstream of the step, on the pressure fluctuations, and the impact of hydrogen addition to the primary fuel (A_{H2f}) in the presence of the transverse air jet as well are now examined. In these tests, the Reynolds number was 6300, with a corresponding average velocity, $\overline{U}$ = 4.4 *m/s*. The primary fuel supply was fixed. The transverse jet air velocity, u_j, was varied from 0-8.4 *m/s*. The hydrogen addition was at 1.6 and 3.2 % of the primary fuel, based on the lower heating value. The baseline equivalence ratio, ϕ=0.57. The overall equivalence ratio ranged from 0.58 to 0.47, depending on the amount of air jet and H2.

Figure 2-14 shows OASPL as a function of momentum ratio of main air to cross jet flow, $\beta = u_j^2 / \overline{U}^2$, at different H2 flow rates. For all cases, the pressure oscillations first increased for $\beta < 0.5$, where they reached a maximum. Above this value, the OASPL dropped rapidly. Without hydrogen, the flame blows out for $\beta < 1.8$. However, with $\beta > 1.8$ the flame became sustainable again, with a pressure reduction of up to 14 *dB* from the baseline case. With air addition, the overall equivalence ratio was mostly below the nominal flammability limit of propane/air mixture. Moreover, a relatively large momentum in the transverse jet was necessary to reduce the pressure fluctuations and stabilize a flame near the step at yet lower equivalence ratio. Thus, it appears that the impact of the transverse jet is aerodynamic. Studies of simple jet in cross flow show that at small velocity ratios, the jet hardly penetrates into the stream, while as the jet velocity increases, the jet penetration is pronounced and its impact is sustained several jet widths downstream [41]. At high velocity ratios, the jet deflects the primary stream upwards, keeping it away from the lower walls. By deflecting the stream away from the lower wall, less heat is lost to the lower wall and combustion is more adiabatic. Since the transverse jet reduces heat loss and lowering the heat loss promotes burning of lean to very lean mixtures [42], the air jet enables burning at a lower overall equivalence ratio.

Figure 2-14 shows that adding H2 to the primary air stream, in the presence of the transverse jet, has a weak impact on the pressure level before the point of maximum pressure oscillation is reached. Beyond this point, the effect of H2 addition is to support a more stable flame, lowering pressure oscillation and preventing blowout. Moreover, adding hydrogen enables burning over the entire range of the jet mass flow rate (we no longer see blowout around β=1). This is consistent with previous observations that doping hydrocarbons with small amounts

of H2 extends their flammability limits and reduces their tendencies to extinguish under the influence of strong strains [26-31]. It is interesting to observe that while 1.6 % H2, measured as a percentage of the primary fuel based on the lower heating value, improves flame stability, doubling that amount did not prove to be more effective.

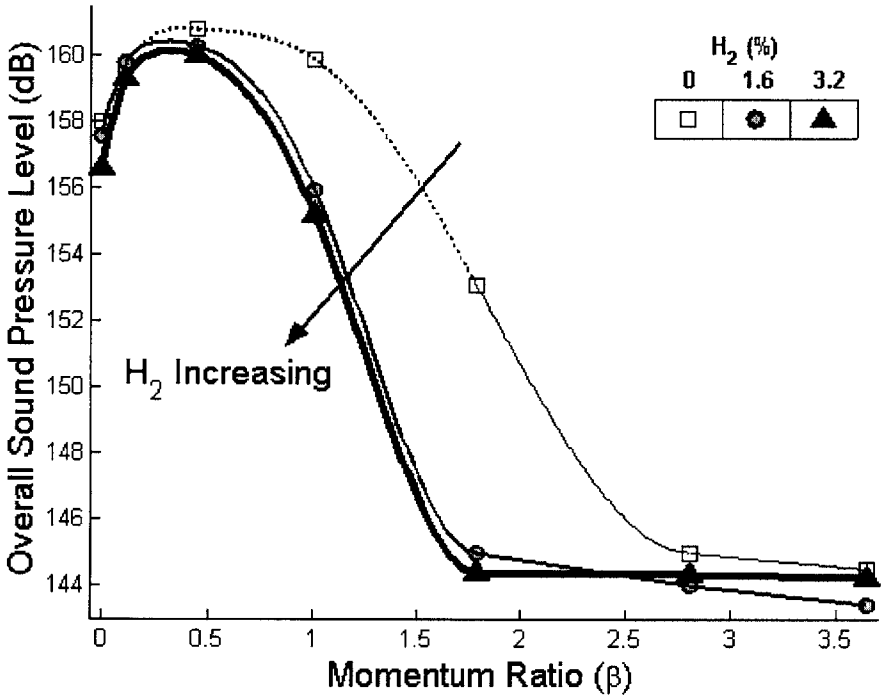

Figure 2-14 Dependence of the Overall Sound Pressure Level on the momentum ratio of the static air injected near the step, for primary air flow velocity of 4.4 *m/s,* and a fixed fuel flow. The overall equivalence ratio ranged from 0.58 to 0.47 depending on the flow rate of the air jet and H2.

Figure 2-15 shows that the introduction of an air jet generally reduces NO levels. The data also show that the impact of the air jet may be non-monotonic when hydrogen is added to the primary fuel; only beyond the point of maximum pressure oscillations does a further increase of the air jet momentum guarantee substantial reduction in NOx. Before that, there is a complex

dependence of NOx on the transverse jet momentum, mostly because of the competing effects of the dynamic flame structure, the equivalence ratio and the temperature fluctuations. Stable combustion, associated with both leaner and more aerodynamically compact flame in the presence of a transverse air jet, leads to a faster drop in NO. As in the case of pressure fluctuations, it appears that high transverse jet momentum is necessary to achieve a measurable reduction in NO formation. Note that hydrogen addition under the same conditions boosts NO levels over the entire range, as the temperature rises in the combustion zone and in the products. Thus, if H2 is to be used to lower the pressure level, it must be supplemented with additional air, to be introduced strategically into the burning zone so as not to jeopardize the emissions.

Figure 2-16 shows the correlation between the NOx level and the OASPL with the change in the momentum ratio of the air jet. It clearly shows that the air jet can simultaneously control combustion instability and emissions. Without H2, the relationship between the NOx level and the OASPL is almost linear. With H2 addition, we were able to increase the primary air flow by extending the flammability limit. As a result, the NO level was reduced even further. In Ref. [43], I showed that one can able to extend the flammability limit by using an air jet and H2 addition to stabilize the flame, all the way down to $\phi = 0.41$. Combustion remained stable, with sub *ppm* NOx and 145 *dB* OASPL. This is ideal for applications requiring low NOx and stable operation without much product after treatment.

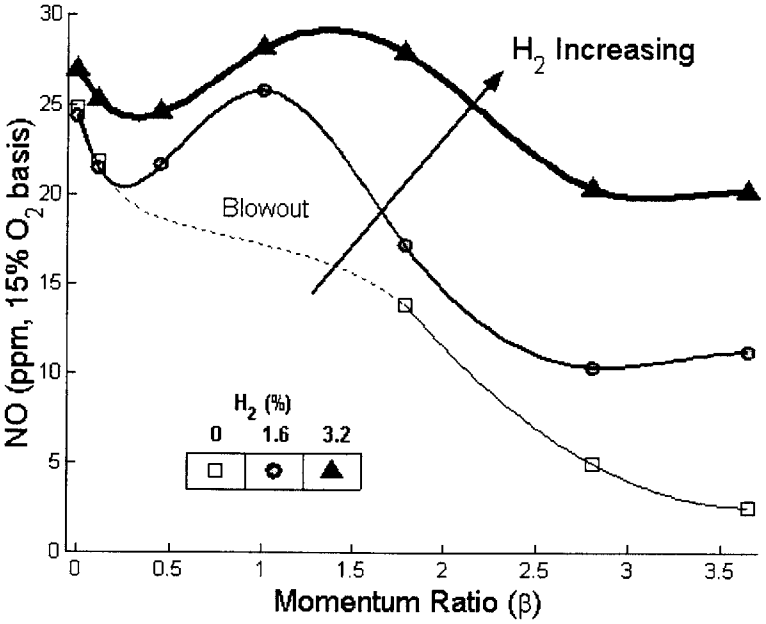

Figure 2-15 NO level dependence on the momentum ratio of the static air jet near the step for primary air flow velocity of 4.4 *m/s*, and a fixed fuel flow. The overall equivalence ratio ranged from 0.58 to 0.47 depending on the flow rate of air jet and H2.

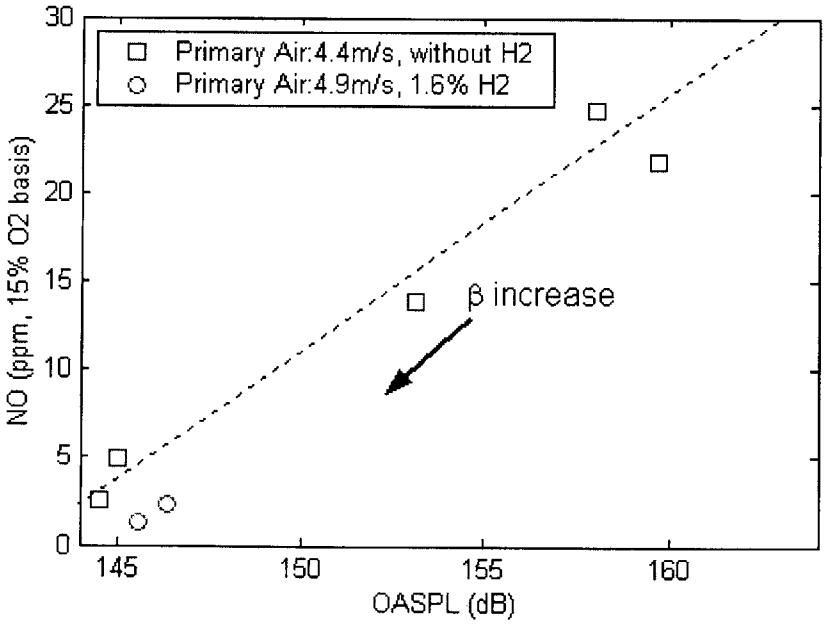

Figure 2-16 Correlations between the Overall Sound Pressure Level and the NO level with changes in the air jet momentum

2.3.2 Modulating the Air Jet (A_{air}) and H2 Injection (A_{H2a}) at the Step

Next, I investigate the impact of the transverse jet modulation on the pressure fluctuations. I show that one advantage of using modulation is to minimize the mass flow rate of the jet by controlling the phase using pressure feedback. I use a phase-shift controller to modulate the mass flow rate of the transverse jet. In these tests, the Reynolds number was fixed at 6300 with a nominal equivalence ratio of 0.57. The momentum ratios were $\beta = 0.64$, 1.56 and 2.89. Pure air, or an air-hydrogen mixture, in which H2 contributed 1.6 % of the total heat addition, were used in the transverse jet. Hydrogen was premixed with air and injected through the slot. With air jet modulation, adding H2 to the transverse jet at the slot was more effective than adding hydrogen to the primary fuel. Paradoxically, without modulation, the opposite was true, i.e. adding H2 to the primary fuel stream was more effective.

To examine the response of combustion dynamics to the transverse jet modulation, I used a simple phase-shift controller with pressure feedback. A high pass filter with a cutoff-frequency at 5 *Hz* was incorporated to eliminate the drift in the pressure measurement and ensure that the duty cycle was always at 50%.

Figure 2-17 shows the OASPL as a function of β and the phase, with pure air injected at the slot. For $\beta > 1.56$ substantial reduction in OASPL could be achieved, but the performance is strongly dependent on the phase. Optimal phase angle in the phase-shift controller was found to be around 200 degrees. In the case with $\beta = 1.56$ the flame blew out at 60 and 120 degrees phase,

as indicated by the dotted line in the figure. This is similar to the results observed previously where a small amount of cross jet was detrimental to stability and caused flame blowout. With β = 2.89 a pressure reduction up to 14 *dB* is realized at the same phase angle of 200. Increasing the air jet velocity to β = 2.89 reduced pressure fluctuations throughout the entire range of phase angles, widened the stability band around 250 degrees and eliminated the flame blowout observed at lower velocities. It is interesting to observe that the maximum pressure reduction is comparable to that obtained with a static transverse air jet, showing some saturation effect. This was also observed in Figure 2-14 where at high velocity ratios, the pressure level reached a plateau. Thus, regardless of the flow rate of the transverse jet, whether it is static or modulated, there appears to be limit on performance.

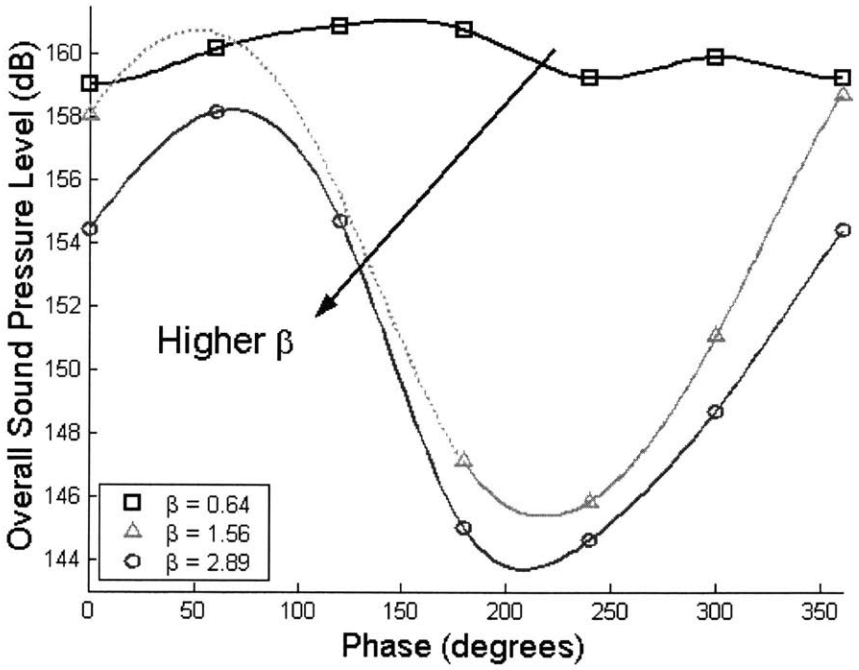

Figure 2-17 Dependence of the Overall Sound Pressure Level on the momentum ratio of the modulated air jet without H2 addition injected near the step and the phase angle, for primary air flow rates of 4.4 *m/s,* and a fixed fuel flow. The overall equivalence ratio ranged from 0.52 to 0.48 depending on the flow rate of the air jet.

Adding H2 in the transverse jet significantly increases the effectiveness of control, as shown in Figure 2-18. With H2 addition, the transverse jet momentum required for flame stabilization dropped by more than one half. By adding H2 at 1.6 % of the total heat-release, the flame was stabilized at a momentum ratio of only 0.64, with a pressure drop up to 13 *dB* from the unstable case. Note that the optimal phase angle is now 300 degree. While a pure air jet reduces the burning velocity, the jet with H2 increases it, and we observed that H2 addition moves the burning zone closer to the step [43].

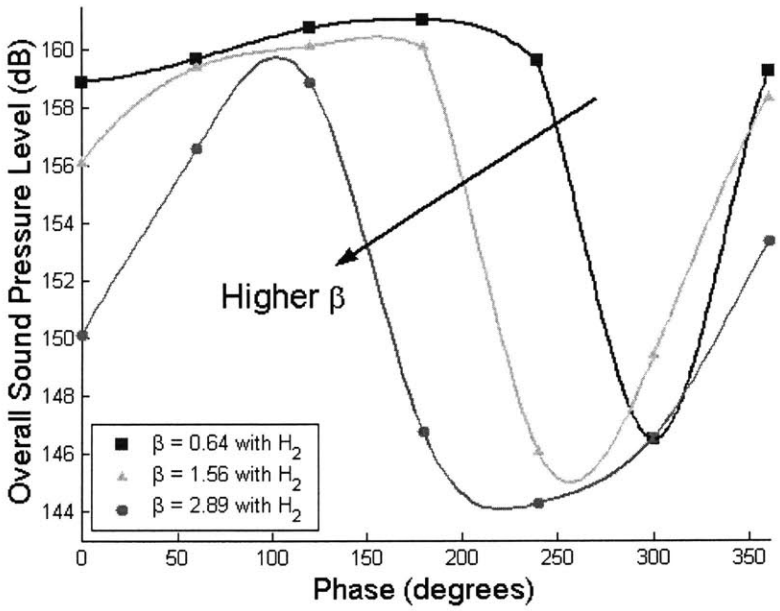

Figure 2-18 Dependence of the Overall Sound Pressure Level on the flow rate of the modulated air jet with H2 addition injected near the step and the phase angle, for primary air flow rates of 4.4 *m/s,* and a fixed fuel flow rate. The overall equivalence ratio ranged from 0.52 to 0.49 depending on the flow rate of the air jet.

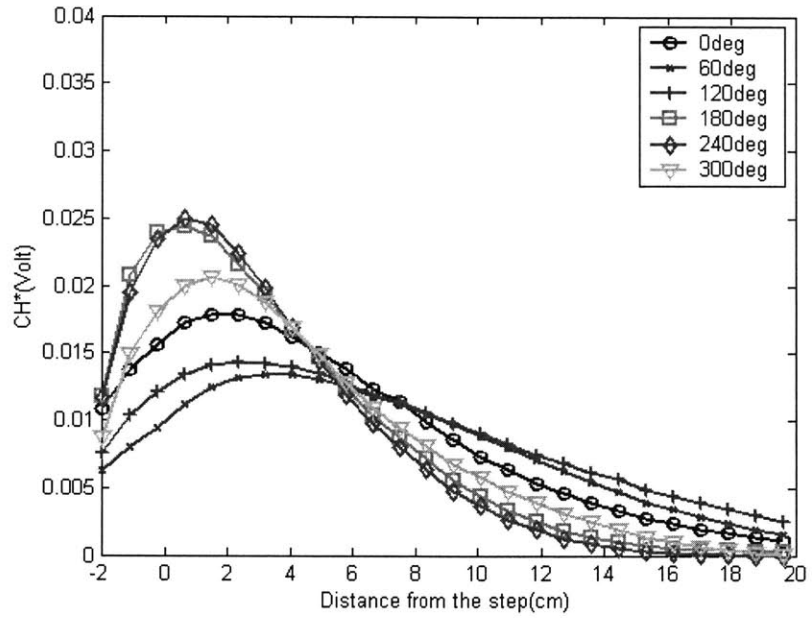

Figure 2-19 Dependence of the mean CH* distributions on the phase angle of the controller for β = 2.89 with the overall equivalence ratio of 0.48 and without H2 addition.

Figure 2-19 shows the mean CH* distribution of the flame for the case of $\beta = 2.89$, over a range of the controller phase angles. Clearly, the burning characteristics change significantly with the phase-shift controller. At the optimal phase angles of 180 and 240 degrees, the burning zone is closest to the step and the burning rate falls rapidly further downstream. In the most unstable case at 60 degree lag, burning extends much further downstream, the peak drops by one half and is located about 2 step heights downstream of the step.

2.4 Summary

In this Chapter, I address emission reduction in addition to instability suppression in a premixed backward-facing step combustor using a transverse air jet near the burning zone, and H2 addition to the air jet. I first develop an insight into the interactions between hydrodynamics, fuel/air mixture inhomogeneity and heat-release dynamics, and their impact on the instability of the combustion system. A parametric study was conducted to investigate the impact of flame-vortex interactions and fuel/air mixture inhomogeneity on the combustion instability. The location of the fuel injection was varied, which changed the total convective time delay and the level of fuel/air mixture inhomogeneity. Results show that when the primary fuel injection is moved further upstream, the impact of fuel/air mixture inhomogeneity is negligible and amplitude of pressure oscillations increase monotonically with increasing the Reynolds number. High-speed CCD images of the flame confirm that a strong flame-vortex interaction is the dominant mechanism for heat release dynamics in all cases. For this reason, I focus the control effort on modifying the flame-vortex interactions in the combustion zone using a transverse jet of pure air or air-hydrogen mixture near the step.

I study experimentally the impact of a static and modulated transverse jet on stability and emissions. I demonstrate that with sufficient momentum, a static air jet injected perpendicular to the incoming flow near the step favorably modifies flame-vortex interactions and reduces pressure oscillations by up to 14 *dB*, while reducing NOx emission by an order of magnitude. I

also investigate the impact of the transverse jet modulation using closed-loop control with pressure feedback. I show that modulating the air jet can achieve the same level of pressure reduction with 50% of the air flow rate required in the static air jet case, but the control effectiveness is strongly dependent on the phase angle. In both cases, adding small amounts of H2 leads to further reduction in OASPL.

3. Modeling and Control of Spatio-temporal Combustion Dynamics

(Configuration II: U. Maryland Axisymmetric Dump Combustor)

Active control of combustion is an enabling technology for operating propulsion systems over a wide range of conditions without running the risk of thermoacoustic instability. In active instability control, the state of the system is determined using point measurements of the pressure and/or the heat release rate, and the signals are used in a control algorithm to determine the output necessary to stabilize the system. Improving the burning characteristics, in addition to the suppression of pressure oscillations, requires a sensing technology that can detect some spatial information, e.g., the spatiotemporal burning distribution. In this Chapter, I explore the application of a new sensing technology described in Section 2.1.1 capable of capturing the spatial properties of the combustion zone as a feedback sensor. The sensor is composed of 128 photodiodes arranged in a row that can capture light intensity up to 3000 *frames/s*. It was tested in a partially premixed 50 *kW* dump combustor exhibiting strong flame-vortex interactions at 38 *Hz*, which coincided with the quarter-wave acoustic mode of the inlet tube. The sensor was used to capture high frequency spatial and temporal combustion fluctuations. To exploit the spatial information as a closed-loop feedback signal, Proper Orthogonal Decomposition (POD) is used to reduce the number of states to a manageable size [44]. The burning characteristics are then described using the amplitude of the first POD mode and a system identification model. Closed-loop control results show that the controller can reduce pressure oscillation by 23 *dB*, while

making the burning zone more compact and bringing it closer to the sudden expansion section. In Section 3.1, I describe the combustor setup. In Section 3.2, I show uncontrolled combustion characteristics using Schlieren and linear photodiode array images. In Section 3.3, reduced-order modeling based on POD and System Identification (SI) is described. In Section 3.4, the control algorithm and its implementation are presented. Finally, closed-loop control results are described in Section 3.5.

3.1 Experimental Setup

The combustor consists of a 4 *cm* circular pipe expanding into a square dump whose height and length are 10 and 61 *cm*, respectively (see Figure 3-1 and Figure 3-2). Ethylene is premixed with the air at flow rates of 0.9 *g/s* and 23 *g/s*, respectively. Two secondary fuel injectors are located at the dump plane, 45 degrees with respect to the flow directions. However, only one fuel injector is used in this experiment. Liquid ethanol is used in the secondary fuel stream at flow rate of 0.15 *g/s*. A pressure sensor is located 5 *cm* downstream from the dump plane actuator. Measurements are recorded using a Keithley MetraByte DAS-1801AO data acquisition and control board hosted in a Pentium I PC.

The schematic diagram of the photodiode array is shown in Figure 3-3. It is composed of 128 photodiodes arranged in a row at spacing of 50 μm with a height of 2.5 *mm*. This sensor has high UV sensitivity with excellent output linearity. The image domain in this experiment is 10 by 14.6 *cm* as shown in Figure 3-3, and 68 of the 128 sensors are used at 500 *frames/sec*. Bi-convex UV fused silica lens with diameter of 25.4 *mm* and f=35 (the lens focal length) is used to project the flame images on the photodiode array. Changing the distance between the lens and the combustion zone can vary the magnification factor. To capture CH* chemiluminescence, which can be correlated with the heat release rate [33,34], a CH* filter centered at 430 *nm* with bandwidth of 8 *nm* is used. To digitize and process the analog signal from the photodiode array, a data acquisition board installed in a Pentium IV computer is used with LabVIEW.

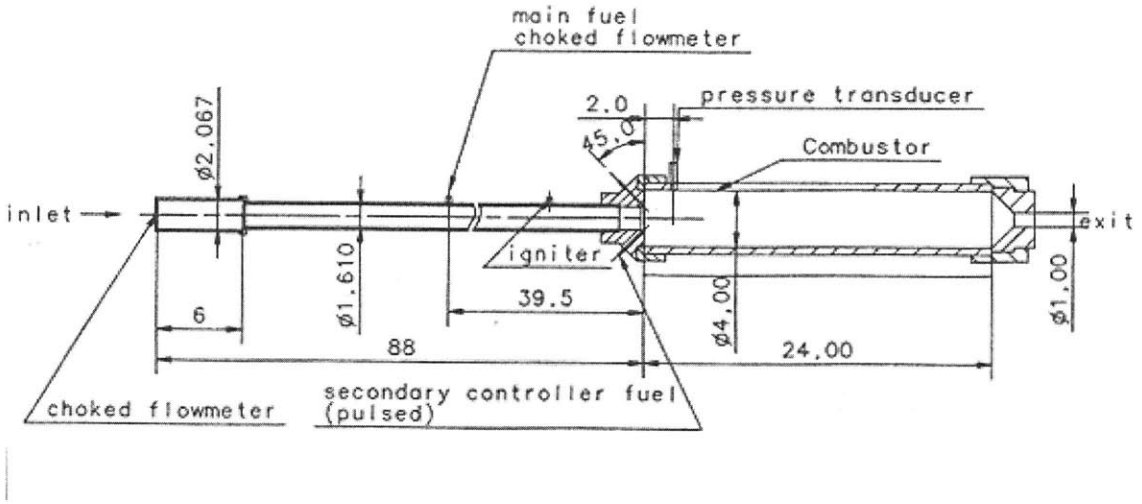

Figure 3-1 Schematic diagram of a dump combustor

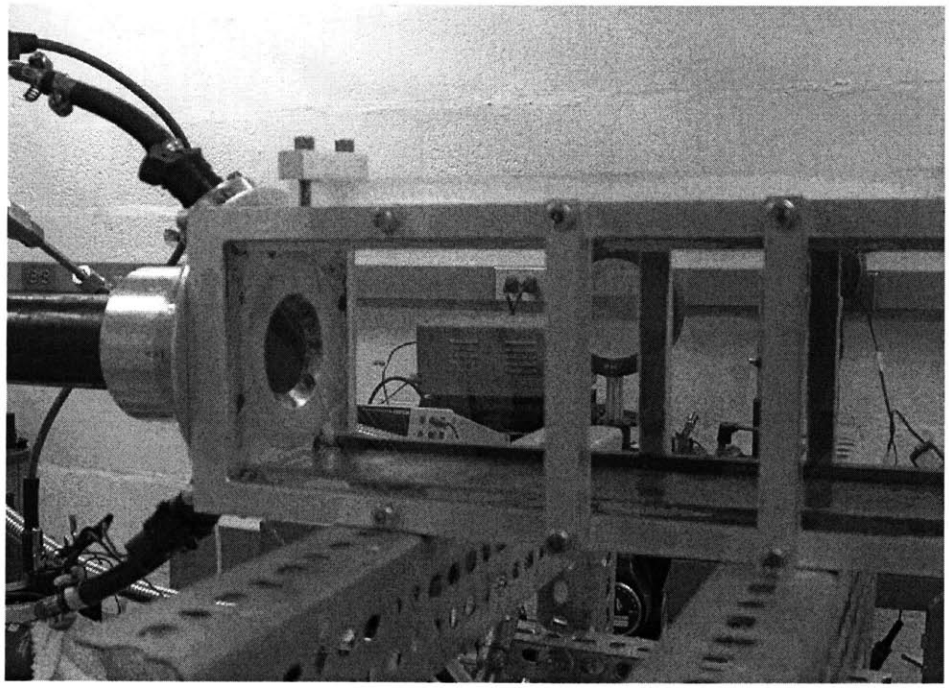

Figure 3-2 A photograph of the dump combustor

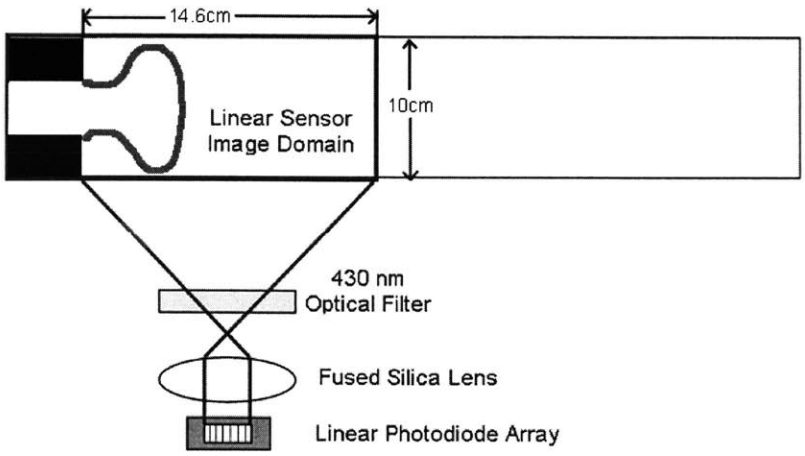

Figure 3-3 The Linear photodiode array arrangement and the imaged area in the combustor.

3.2 Uncontrolled Combustion Characteristics (Flame-Vortex Interactions)

The combustor was naturally unstable at equivalence ratio ϕ=0.6 and air flow rate of 23 *g/s*. At this condition, the fundamental mode was 38-40 *Hz* along with several higher harmonics. The frequency of the fundamental mode coincided with the quarter-wave acoustic mode of the inlet tube. Due to the location of the main fuel injection, 1 *m* upstream of the step, the impact of equivalence ratio oscillations on the heat release dynamics and its coupling with the acoustics leading to the combustion instability is expected to be small. Instead, the Schlieren images in Figure 3-4 show the flame wrapped around a large-scale structure, which is periodically shed near the expansion section. Although the detailed mushroom-shaped flame front is not clearly shown, due to the presence of small-scale structures and the wall effects, a large-scale flame structure in the middle of the domain can be easily identified.

From measurements using the linear photodiode array at different phase angles, depicted in Figure 3-5, one can correlate the heat release fluctuation with the large-scale flame structure; the periodic vortex shedding, and its convection to downstream. Note that the photodiode array is primarily a 1-D sensor; it integrates the signal in the cross stream direction. The convective velocity of the large-scale structure identified in Figure 3-5 can be estimated from the slope of the line connecting the maximum CH* points at different phase angles. For the case analyzed here, this velocity is 10 *m/s* which corresponds to the mean velocity of the flow (note that the 360° on the x-axis corresponds to 25 *ms*.). The existence of a large scale structure, which is

captured in the Schlieren images and the linear photodiode array data in Figure 3-4 and Figure 3-5, makes it possible to develop a reduced-order model representing the spatio-temporal heat release characteristics, using POD analysis, as will be done in the next section.

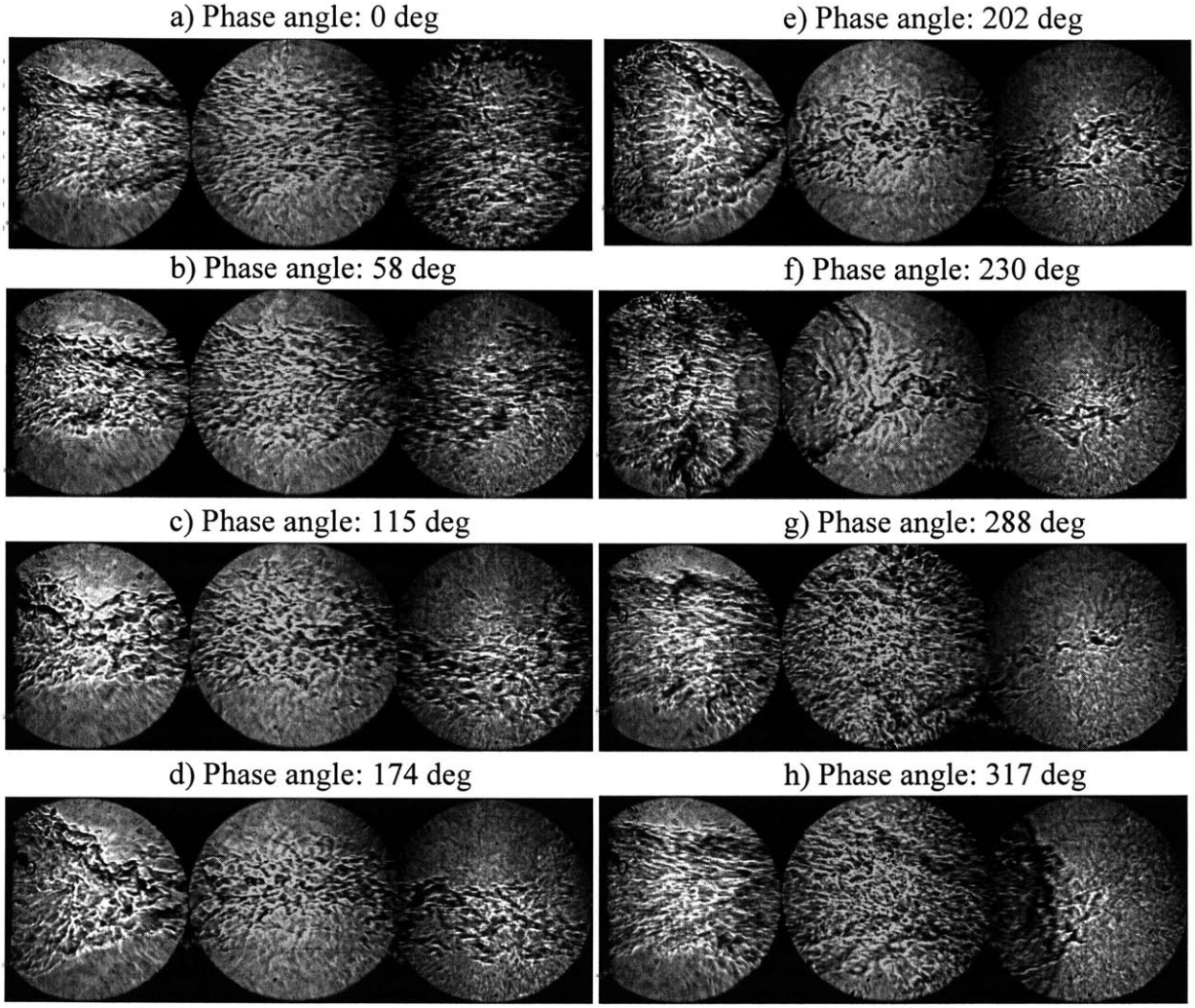

Figure 3-4 Schlieren images at different phase angles (0 degree corresponds to the maximum pressure). The domain of the Schlieren image is 20.2 *cm* × 7.5 *cm*.

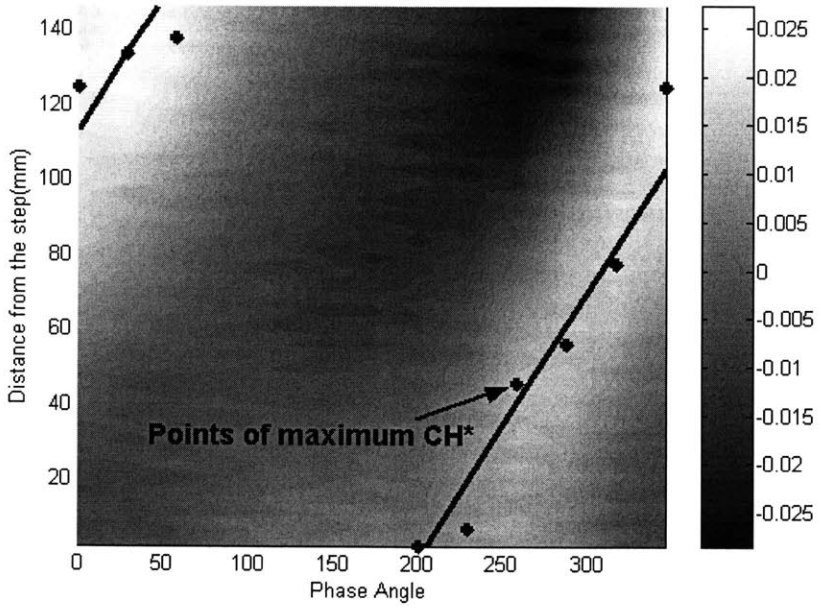

Figure 3-5 Measured CH* fluctuations using the photodiode array at different phase angles (0 phase angle corresponds to pressure maximum). The viewing window is 100 × 146 *mm*.

3.3 Reduced Order Modeling Using POD and System Identification

To develop a model that can capture the spatio-temporal variation of the heat release due to the control input, Proper Orthogonal Decomposition (POD) is used to systematically extract the most energetic modes. These modes are used as basis functions for a System Identification based model in order to reduce the solution space to the smallest linear subspace that is sufficient to describe the system [45].

3.3.1 Proper Orthogonal Decomposition (POD)

Proper Orthogonal Decomposition (POD) is a systematic approach for extracting the most energetic modes from a set of realizations obtained from the plant model. These modes can be used as basis functions for Galerkin projections of the governing equations in order to reduce the solution space to the smallest linear subspace that is sufficient to describe the system. The decomposition is 'optimal' in that a N-ordered POD base corresponds to the smallest projection error compared to any other N-ordered base in a mean-squared sense. Over the years, it has been applied in several disciplines including fluid mechanics, stochastic processes, image processing, signal analysis, data compression, process identification and control in chemical engineering, and oceanography. Particularly in fluid mechanics, the POD technique has been applied in the analysis of coherent structures in turbulent flows and in obtaining reduced order models to describe the characteristics of the associated phenomena [44].

Ravindran [46] developed a POD and Galerkin projection based reduced order model for minimizing the vorticity level of a backward facing step flow using blowing on the step corner. The set of realizations for deriving POD basis was obtained from a finite element analysis of the flow by considering solutions to the controlled problem with appropriate control inputs. The author found that POD provides a systematic way to improve accuracy of the reduced model while maintaining well-conditioned system matrices, when compared to other reduced order techniques. Graham *et al.* [47,48] investigated the application of low-order models (using POD and Galerkin projection) to control of the unsteadiness in a cylinder wake by changing the cylinder rotational speed. The authors demonstrated that a poor choice of the set of realizations for computing the basis functions of the low-order model can negate the benefits of control and cause unsteadiness to rise. The technique to choose the 'right' basis function was left as an open question by the authors. The process of reducing the plant model order using POD and designing a controller that takes the system from its original state towards its optimal state does not guarantee that the reduced order process will converge to the optimal control of the original (large) system. Arian *et al.* [49] established convergence of the POD-based reduced-order technique in the presence of control input, by embedding it into the concept of Trust-Region (TR) methods. Most of these researches are through simulations due to the difficulty of processing large amount of data in real time. Here, I apply this POD technique to a combustion control problem using the linear photodiode array and validate it in a 50kW dump combustor. One problem that arises when using POD algorithms in closed-loop control is that the modal shape can change due to the control input. To overcome this difficulty, I use the Recursive POD

(RePOD) to recursively updated the POD mode online [50]. I first summarize the standard POD method and subsequently introduce the RePOD algorithm.

The POD Algorithm

If $Q'(x,t)$ is a zero-mean variable, then the POD method seeks to generate an approximation for Q' by using separation of variables as

$$\hat{Q}'(x,t) = \sum_{i=1}^{l} a_i(t)\phi_i(x)$$

where $a_i(t)$ is the ith temporal amplitude, $\phi_i(x)$ is the ith spatial basis function, l is the number of modes chosen, and t and x are the temporal and spatial variables, respectively.

The set of realizations from a plant required for the POD basis calculation is typically obtained experimentally or computationally and as such is discrete in nature. So, what follows in this section refers to discrete nature of the variables concerned.

Let m be the number of temporal points in the data ensemble, and n be the number of spatial points. The POD method consists of finding ϕ_i (x) such that the projection error $Q'(x,t) - \hat{Q}'(x,t)$ is minimized. This optimization problem can be stated as follows. Denote $\{\phi_i(x)\}_{x=x_1,\ldots,x_n} = \phi_i \in \Re^n$, $i = 1,\cdots,l$. The optimization problem is then given by:

$$\underset{\phi}{Min}\, J_m(\phi_1,\cdots,\phi_l) = \sum_{j=1}^{m} \left\| Q'_j - \sum_{k=1}^{l} (Q'^T_j \phi_k)\phi_k \right\|^2$$

$$\text{subject to: } \phi_i^T \phi_j = \delta_{ij}, 1 \le i, j \le l, \phi = [\phi_1, \cdots \phi_l]$$

where $Q'_j \in \Re^n$ is the vector of variable Q' at time $t = t_j$, i.e., $Q'_j = \{Q'(x_1, t_j), \cdots, Q'(x_n, t_j)\}$. Also, $\left(Q_j'^T \phi_k\right)$ in the cost function is the k[th] temporal amplitude a_k at time t_j. So the expression within the first summation sign is $\left\| Q'_j - \sum_{k=1}^{l} a_k \phi_k \right\|^2$ which refers to the projection error for the data Q'_j.

The POD modal set can be obtained using the 'method of snapshots' as follow [51,52]. Denote $Q'_j(x_k) = Q'(x_k, t_j)$. Also, let the matrix Y be formed as follows: $Y = [Q'_1, \cdots, Q'_m]$. Then, a singular value decomposition of the matrix Y gives : $Y = B\Sigma A^T$, where A and B are unitary matrices, and

$$\Sigma = \begin{bmatrix} \sigma_1 & & & \\ & \sigma_2 & & \\ & & \ddots & \\ & & & \sigma_l \end{bmatrix}, \sigma_1 \ge \sigma_2 \ge \cdots \ge \sigma_l .$$

Then

$$\phi_i(x_k) = \sum_{j=1}^{m} \frac{A(j,i) Q'_j(x_k)}{\sigma_i}, i = 1, \cdots, l; k = 1, \cdots, n.$$

The eigenvalues corresponding to the POD modes are the squares of the singular values $\{\sigma_1^2, \sigma_2^2, \cdots, \sigma_l^2\}$, and represent the 'energy content' of the modes. Next we consider Recursive POD (RePOD) to updated the POD modes online.

The RePOD Algorithm

Suppose we begin at time t_m, with $\phi^{(m)}$, where $\phi^{(m)}$ represent the POD modes at time t_m. Given a new measurement Q'_{m+1} at time t_{m+1}, we seek to minimize ΔJ, defined as

$$\underset{\phi}{Min}\,\Delta J(\phi_1,\cdots,\phi_l)=\left\|Q'_{m+1}-\sum_{k=1}^{l}\left(Q'^{T}_{m+1}\phi_k\right)\phi_k\right\|^2 \qquad \text{Eq.(3-1)}$$

$$\text{subject to: } \phi_i^T\phi_j=\delta_{i,j},\ 1\le i,\ j\le l,\ \phi=[\phi_1,\cdots,\phi_l]$$

The assumption is that with the addition of the new data set, the number of POD modes does not change.

Equation (3-1) can be solved as follows:

Step 1: Find $\phi_1^{(m+1)}$ that minimizes $\Delta J^{(1)}=\left\|Q'_{m+1}-\left(Q'^{T}_{m+1}\phi_1\right)\phi_1\right\|^2$ over all ϕ_1 under condition that $\phi_1^T\phi_1=1$.

Step i: Using the values of $\phi_1^{(m+1)},\cdots,\phi_{i-1}^{(m+1)}$, find $\phi_i^{(m+1)}$ that minimizes the overall ϕ_i,

$$\Delta J^{(i)}=\left\|Q'_{m+1}-\sum_{k=1}^{i-1}\left(Q'^{T}_{m+1}\phi_k^{(m+1)}\right)\phi_k^{(m+1)}-\left(Q'^{T}_{m+1}\phi_i\right)\phi_i\right\|^2.$$

Normalize $\phi_i^{(m+1)}$. Continue for $i=2,\cdots,l$.

The minimization of $\Delta J^{(i)}$ in Step i can be carried out using gradient techniques:

$$\phi_i^{(m+1)}=\phi_i^{(m)}-\delta\left.\frac{\partial\Delta J^{(i)}}{\partial\phi_i}\right|_{\beta>0}$$

$$\phi_i^{(m+1)} = \phi_i^{(m)} + \delta\{Q_{m+1} - (\sum_{k=1}^{j-1}(Q_{m+1}^T \phi_k^{(m+1)})\phi_k^{(m+1)} + +(Q_{m+1}^T \phi_i^{(m)})\phi_i^{(m)})\}(Q_{m+1}^T \phi_i^{(m)}) \qquad \text{Eq.(3-2)}$$

Equation (3-2) is the RePOD algorithm. While this does not guarantee orthogonality of ϕ_i^m at each time t_m, it leads to an orthonormal set of modes as $t \to \infty$. This RePOD algorithm is used with closed-loop control when the combustion dynamics is expected to change drastically and results are in Section 3.5.

Results

In the POD analysis, 500 consecutive photodiode array images (m = 500) were used. The number of sensors used was 68 out of 128 (n = 68) and the sampling rate was 500 *frame/sec*. To match the overall equivalence ratio with the controlled case, a white noise signal was sent to the secondary fuel injector with a duty ratio of 50%. The results are depicted from Figure 3-6 to Figure 3-8. Figure 3-6 shows that the first and second modes contain almost 60 % and 30 % of the total energy, respectively, indicating that with one or two basis functions one can accurately describe the spatial variations of heat release. The shapes of the basis functions are shown in Figure 3-7, with the frequency spectrum of modal amplitudes in Figure 3-8. The first two modes correspond mainly to the flame oscillation at around 40 *Hz* and the other two modes to 40 and 80 *Hz*.

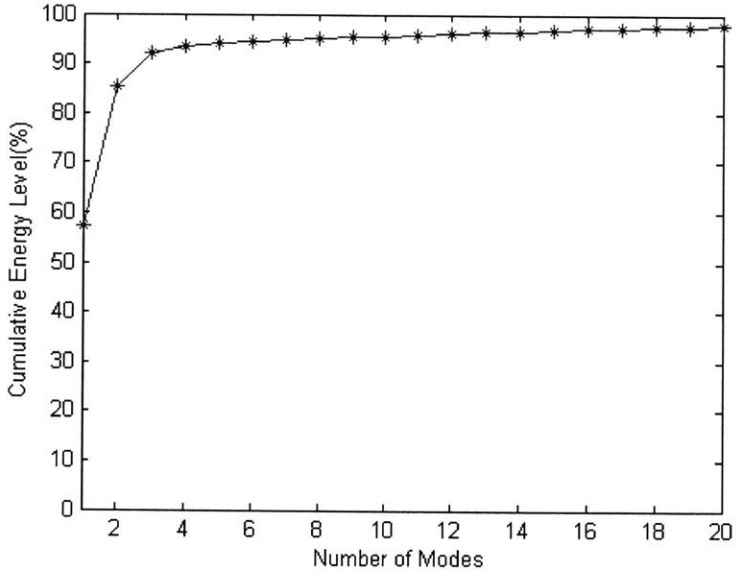

Figure 3-6 Cumulative energy in the POD modes

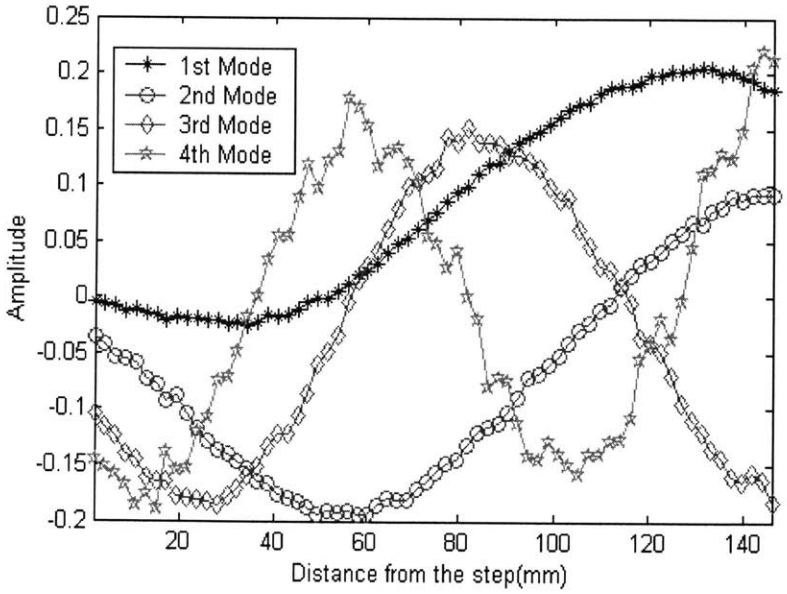

Figure 3-7 The first four POD mode shapes

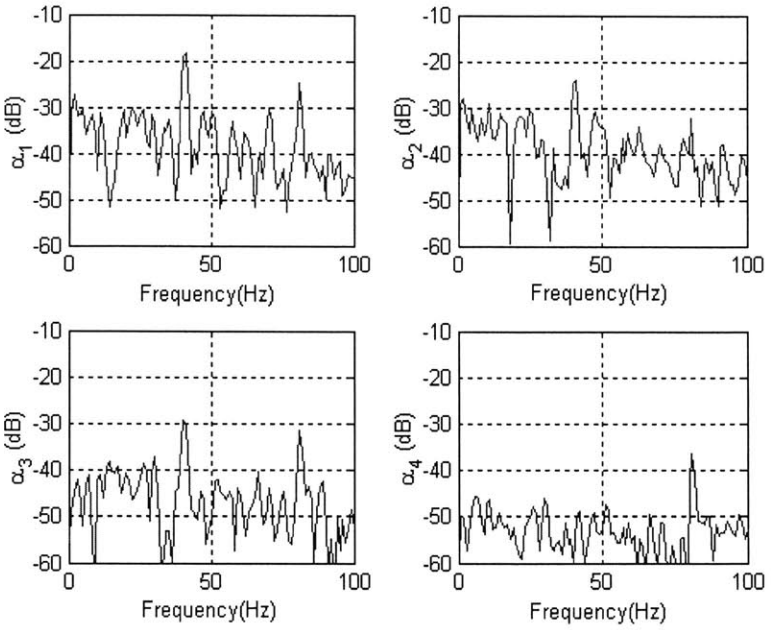

Figure 3-8 The power spectral densities of the modal amplitudes

3.3.2 System Identification

POD is an "empirical" method applied to determine the basis functions by examining the highest existing correlations. The Navier-Stokes equation could then be projected onto these basis function spaces to obtain reduced order models. However, studies showed that this projection suffers from many problems, such as unknown boundary conditions, insufficient damping when smaller scales are neglected, mathematical complexities in the reacting flow case, and numerical errors generated by differentiation. Alternative methods to develop reduced order models have been attempted by Jeong [53] and Gillies [54]. Jeong used POD to generate basis functions in wind-induced pressure on a low-rise building, and applied auto Regressive (AR)

models to fit the response of first 4 modes. Gillies used POD and neural network to furnish an empirical prediction of the modal response of the wake to external forcing, in a flow past a circular cylinder. I use a similar approach as Jeong and Gillies's to develop a reduced order model for the problem under consideration.

To perform SI, a white noise signal was generated, filtered by a band pass filter with a bandwidth of 10-100 *Hz,* and transformed into a binary signal. This signal was sent to the secondary fuel injector, and also used to trigger the photodiode array. Using α_1, the amplitude of the 1st POD mode, as the output and V, the fuel injector signal, as the input, as shown in Figure 3-9, an SI model was developed using a linear AutoRegressive with external input (ARX) model-structure [55] and the time delay, τ_{tot}, was found to be 2 *ms*. The resulting transfer function is shown as follow

$$G_p(s) = \frac{\alpha_1}{V} = \frac{0.00187s^3 + 22.51s^2 + 1.303 \cdot 10^4 s + 6.116 \cdot 10^6}{s^4 + 78.68s^3 + 3.406 \cdot 10^5 s^2 + 1.229 \cdot 10^7 s + 1.707 \cdot 10^{10}} \exp(-0.002s) \qquad \text{Eq.(3-3)}$$

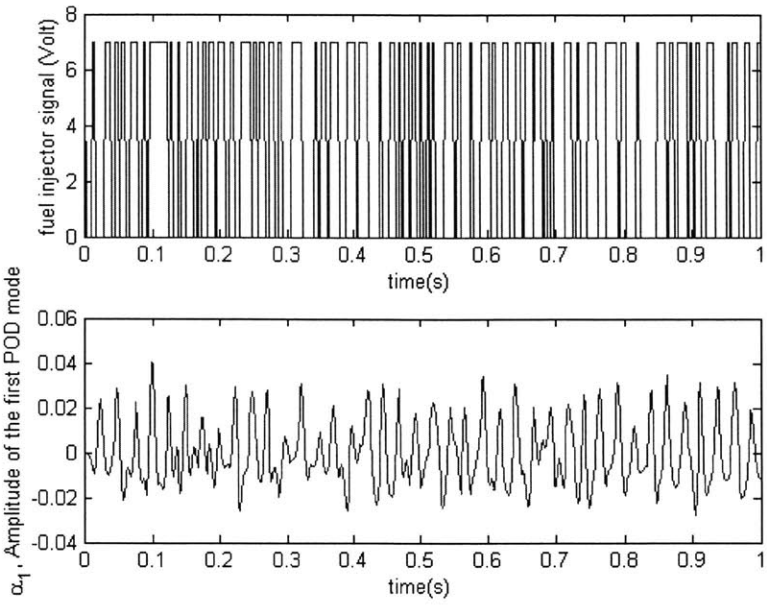

Figure 3-9 Input and output data for system identification: the input, α_1, is the amplitude of the first POD mode, and the output is fuel injector signal.

3.4 Closed-loop Control

3.4.1 Algorithms

A model-based controller called adaptive Posicast was used for pressure stabilization. The adaptive Posicast controller has been developed to stabilize dynamic systems with large time delays [22], by predicting the future pressure response in order to eliminate the delay effects on the closed-loop and using an adaptive algorithm to adjust its parameters. It attempts to predict future outputs using a Smith Controller, and uses a phase lead compensator to drive the future output (parameter fluctuation) to zero. The controller implemented is a discrete form, where the Smith Controller is a finite time discrete integration multiplied by a weighting function (discretized as λ_j). The controller updates the control signal, V(t), as

$$V(t) = k^T(t)d(t) + \dot{k}^T(t)d_a(t) \qquad \text{Eq.(3-4)}$$

$$\dot{k}(t) = -sign(k_o)\alpha_1(t)\Gamma d(t - \tau_{tot}), \qquad \text{Eq.(3-5)}$$

where $k(t)$ and $d(t)$ are the controller parameters and data vectors, respectively and defined as

$$k^T(t) = [-k_1 \quad -k_2 \quad \lambda_n(t) \quad \cdots \quad \lambda_1(t)]$$

$$d^T(t) = [\alpha_1(t) \quad V_c(t) \quad V(t - ndt) \quad \cdots \quad V(t - dt)]$$

where $V_c(t) = \frac{1}{s + z_c} V(t)$, k_o is the high frequency gain of $G_p(s)$, Γ is the diagonal matrix whose diagonal values, γ_1, γ_2, ..., γ_{n+2}, are the adaptation gains, $\lambda_1 \cdots \lambda_n$ are the Smith controller

components to eliminate the delay from the closed loop and $d_a(t) = \frac{1}{s+a} d(t)$. n is determined by the time delay, τ_{tot}, in the SI model $G_p(s)$, $ndt = \tau_{tot}$, where dt is the time step. k_1, k_2, and z_c are components of the phase lead compensator $k_1 \frac{z_c}{s + z_c + k_2}$. z_c is selected to stabilize the unstable mode of the delay free system, while k_1 and k_2 are determined by the adaptation law. The control signal from the

POD is needed to generate the amplitude of the first mode for use in the Posicast controller. However, POD modes will generally change in response to control action, so it is necessary to update them. The POD method involves batch processing past data, and is not feasible in real time. Therefore, a recursive POD (RePOD) method described in 3.3.1 is used in closed control cases.

3.4.2 Implementation

Flame images were first captured by the linear photodiode array at 500 *frames/s* using LabVIEW in the Pentium IV computer. The amplitude of the first POD mode, α_1, was computed by projecting the captured images onto the first POD mode shown in Figure 3-7, and α_1 was used as an input in the adaptive Posicast controller in Eq. (3-4) to generate a control signal for the fuel valve. Finally, the first POD mode was updated using Eq. (3-2).

3.5 Results

The controller described in Section 3.4 was implemented and the results are shown from Figure 3-10 to Figure 3-13. Figure 3-10 shows the pressure response without and with closed-loop control. In the baseline case, the standard pressure level (SPL) reached 155 *dB* at 38 *Hz,* with its harmonic at 76 *Hz,* whose amplitude is as strong as that of the primary. Open-loop modulation in the secondary fuel injector, at 50 *Hz,* decreased the pressure amplitude at 38 *Hz* slightly. Openloop forcing at different frequencies ranging from 10 to 40 *Hz* was also attempted without significant improvement. Next, closed-loop control was used with and without POD adaptation. It resulted in pressure reduction by 18-23 *dB* at the primary mode and complete stabilization in its harmonic. Closed-loop control with POD adaptation led to 5 *dB* more reduction in the primary unstable mode. The adaptation gain, δ, used in the POD adaptation was 0.2.

The impact of the gain, δ, was also examined. Figure 3-11 shows the pressure time response with different POD adaptation gains. A moving window containing 10 previous pressure cycles computed the OverAll Sound Pressure Level (OASPL) at a given time in that figure. For all cases, the controller was turned on at t=1 s. Without POD adaptation (δ=0), fluctuations in the pressure around at 1 *Hz* with 2 *dB* amplitude is observed 2 *s* after the controller was turned on. With δ = 0.1, the pressure drop during $1 < t < 2$ is relatively slow compared to the no-adaptation case. However, pressure fluctuations after t = 2 are lower than in

the no-adaptation case. Finally, with δ=10, the pressure drop during $1 < t < 2$ is fastest, with a small overshoots during $2 < t < 6$ due to the high adaptation gain.

The heat release distribution can change with control. This can be easily identified using the photodiode array, as shown in Figure 3-12 and Figure 3-13. The maximum average CH* emission level was doubled with closed-loop control within the photodiode array domain, with its peak moving closer to the step, as shown in Figure 3-12. Note that the fuel and air flow rates were the same in three cases. Figure 3-13 shows the distributions of the normalized CH* emission fluctuation levels, $Q'_{i,rms} / \overline{Q}_i$, where $Q'_{i,rms}$ is the rms and $\overline{Q}_i$ is the mean value of the i^{th} photodiode with a 1 *s* time window and i=1...68, with and without control. Clearly, the maximum fluctuation point is also shifted upstream significantly, more than 5 step height. The point of the maximum fluctuation in the uncontrolled case was observed at the end of the viewing window, 146 *cm* downstream from the step. However, in the controlled case, the maximum fluctuation occurs very close to the expansion section. Also, there is a slight improvement in the compactness of the burning zone with POD adaptation.

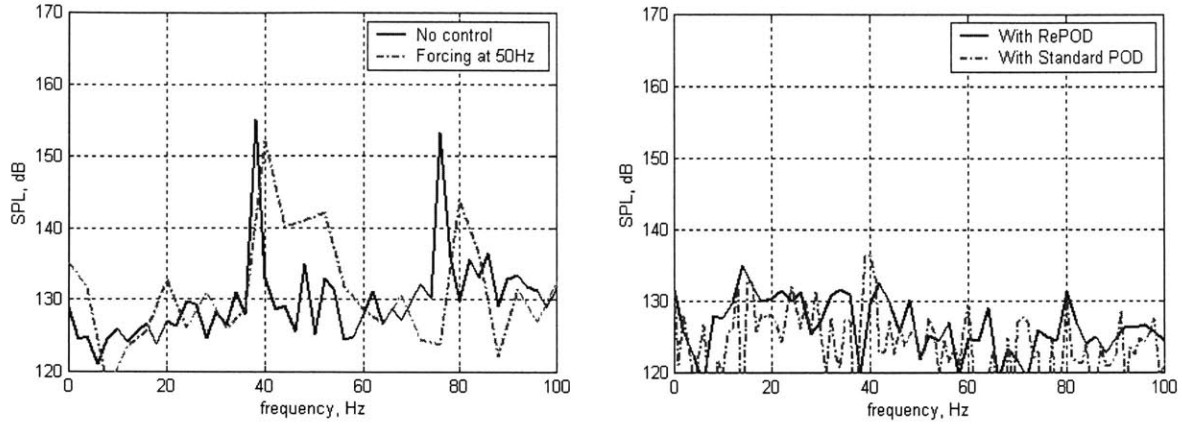

(a) (b)

Figure 3-10 The pressure spectra with and without closed-loop control.

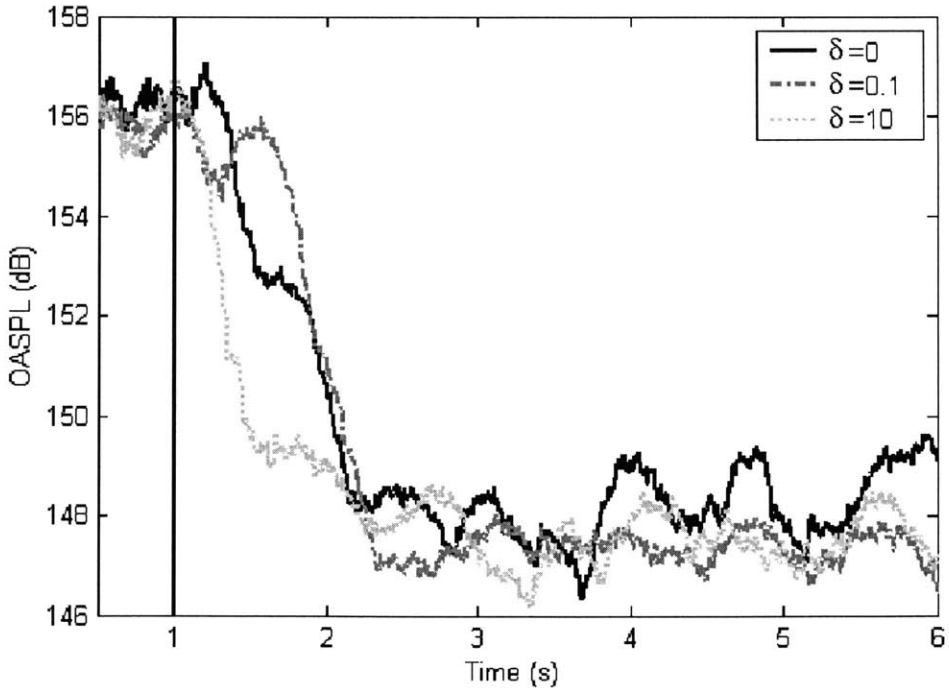

Figure 3-11 Time history of the overall sound pressure level (OASPL) with and without POD mode adaptation. OASPL is calculated from the pressure signal using a moving window containing 10 pressure cycles (128 samples).

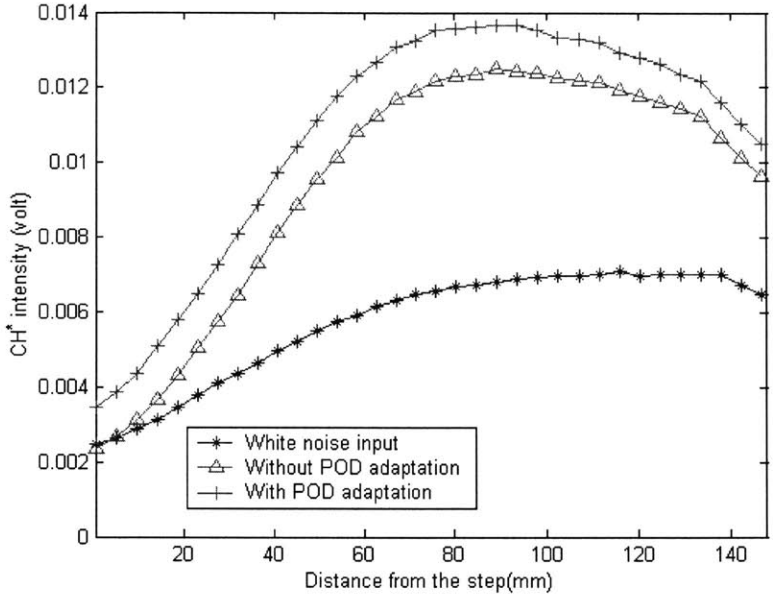

Figure 3-12 Mean CH^* emission with and without control

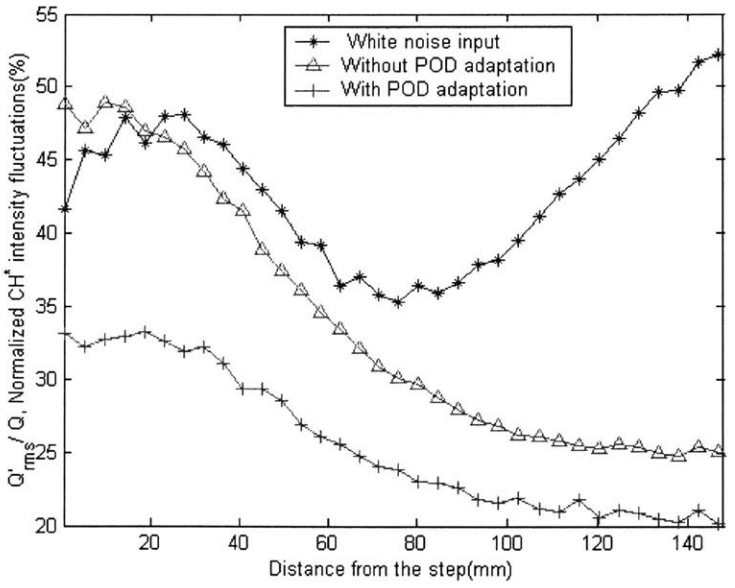

Figure 3-13 The normalized CH* intensity fluctuations, $Q'_{i,rms} / \overline{Q}_i$, using a 1 *s* time window with and without control. $\overline{Q}_i$ is taken from Figure 3-12.

3.6 Summary

In this Chapter, I investigated a sensing technology capable of capturing the spatial properties of the combustion zone. A linear photodiode array which can capture high speed spatio-temporal heat release fluctuations has been tested as a feedback sensor in a 50 *kW* dump combustor. Pressure measurements identified strong oscillations at 38 *Hz*, which is the quarter-wave acoustic mode of the inlet tube. Images taken using the linear photodiode array and a Schlieren system showed large-scale flame oscillations due to strong flame-vortex interactions at 38 Hz. The vortical structures are convected downstream at a speed of 10 m/s. To develop a model of this combustion system, Proper Orthogonal Decomposition (POD) is used to systematically extract the most energetic modes with the first and second POD modes capturing about 60 and 30% of the total fluctuations, respectively. The first mode is used as a basis function for a system identification based model. A model-based controller called adaptive Posicast was used for pressure stabilization, which resulted in pressure reduction of up to 23 *dB*. Heat release characteristics, determined using CH* emission, showed that the maximum value is doubled due to the action of control, and the burning zone moved closer to the step. It should be noted that this model-based controller, as will be shown in Chapter 4, is capable of accommodating on-line changes in the operating conditions of the combustor.

4. Control of Industrial Swirl Stabilized Combustor

(Configuration III: U. Cambridge Swirl Stabilized Combustor)

In this Chapter, I apply the active control strategy in more realistic gas turbine conditions. The design of the rig is based on the primary stage of the Rolls-Royce RB211-DLE industrial gas turbine. To verify whether the strategy is effective across all regimes of plant operation, robustness studies with respect to changes in the resonant frequency, total time delays, changes in operating conditions and initial conditions of control parameters are made. Control is achieved by modulating the fuel flow rate in response to a measured pressure signal and the controller used is the adaptive Posicast described in Section 3.4.1. The controller achieves a reduction of up to 30 *dB* on the primary instability frequency. This performance was an improvement of 5-15 *dB* over an empirical control strategy (simple phase-shift controller) specifically tuned to the same operating point. Robustness studies have shown that the controller retains control for a 20% change in frequency and a 23% change in air mass flow rate. Section 4.1 describes the combustor setup. Section 4.2 discusses the uncontrolled combustion dynamics. Closed-loop control results are in Section 4.3. Finally, robust studies are in Section 4.4.

4.1 Experimental Setup

4.1.1 Combustor

The facility is a generic combustor designed to model the fuel injection/premix ducts of a Rolls-Royce RB211-DLE industrial gas turbine. The swirler unit is a scale model, however the geometry of the plenum and combustor has been reduced to simple cylindrical pipes to have well-defined acoustic boundary conditions. A schematic of the working section is shown in Figure 4-1.

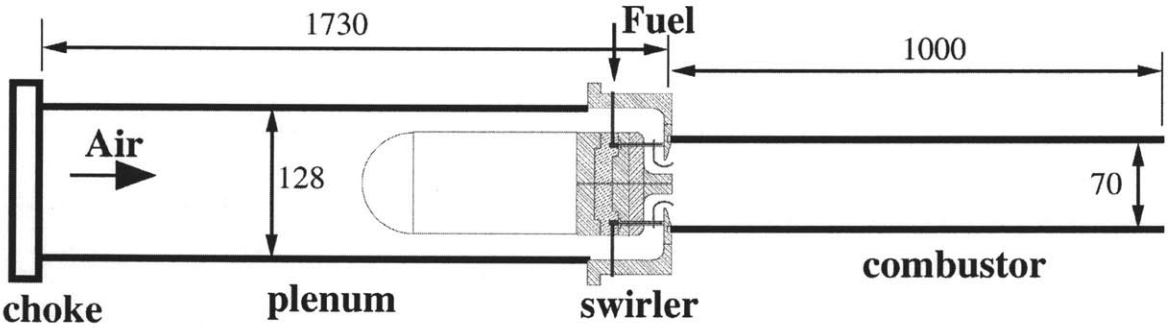

Figure 4-1 Schematic of the rig downstream of the choke plate, showing the plenum/combustion chambers and the swirler unit. All dimensions in *mm*, diagram not to scale.

A metered and steady air flow is supplied to the plenum (128 *mm* ID) through a choked plate. This effectively decouples the air supply from pressure fluctuations in the working section, enabling air to be supplied at a constant mass flow rate (m_a) and providing a well-defined acoustic boundary condition. The maximum mass flow rate available is approximately 0.2 *kg/s*, however the typical operating range is 0.03-0.08 *kg/s*. The downstream end of the plenum

chamber incorporates an annular section prior to the swirler unit. The swirler exit is connected to a quartz tube (70 *mm* ID) along which combustion takes place. This provides ideal optical access to the flame region. The exit of the tube is open to atmospheric pressure and is not choked.

The fuel (ethylene, C_2H_4) and air are mixed using a Rolls-Royce DLE counter-rotating, radial swirler unit, scaled to fit the existing facilities (approx. 54%). Once the airflow has passed into the annular section, it is split into two streams that flow through concentric channels. In the channels, blades are fixed to induce two counter-rotating flows. The fuel is injected upstream into the annular channels through eight cylindrical bars each fitted with two exit holes of 1.0 *mm* diameter (see Figure 4-2) A pressurized commercial cylinder is used to supply the fuel for the swirler unit. The fuel line comprises a pressure regulator, control valve and turbine flow meter (see Figure 4-3). Together with suitably located pressure transducers and thermocouples, the turbine flow meter is used to provide a mass flow reading. Fuel mass flow rates (m_f) are in the range 1.6-3.0 *g/s* in order to obtain equivalence ratios from 0.5-1.0 for the air mass flow rates used in these tests.

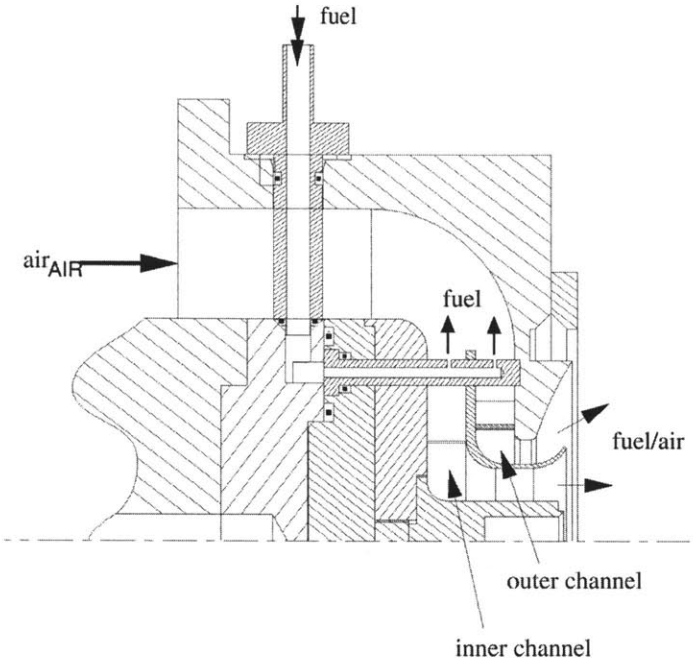

Figure 4-2 Detailed schematic showing a cross-section of the swirler unit and the orientation of the fuel injection bars.

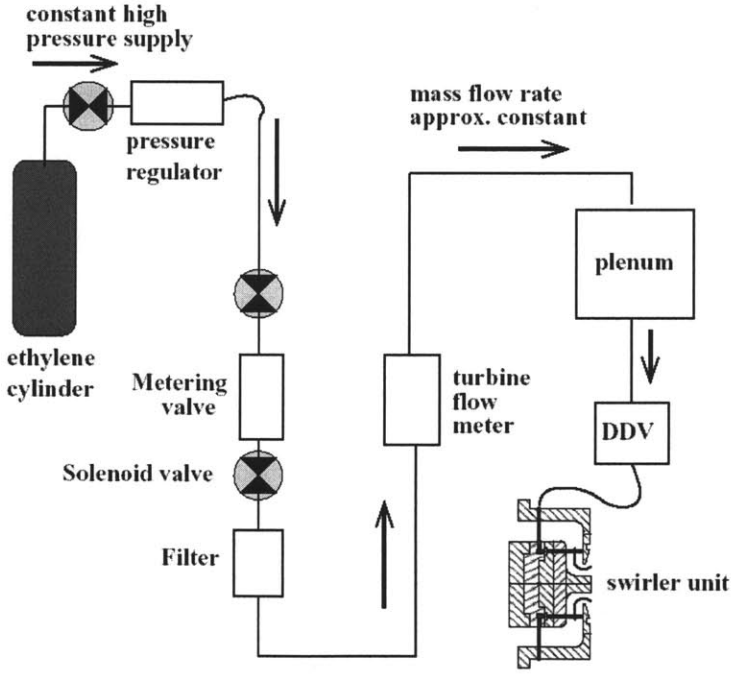

Figure 4-3 Detailed schematic of the fuel system, together with the DDV and the plenum chamber

4.1.2 Instrumentation and Actuation

The feedback signal for the control algorithms is provided by a Kistler piezo-electric pressure transducer (type 601A) measuring combustor pressure 700 *mm* downstream of the swirler unit. The transducer is located in a side arm, 30 *mm* from the combustor wall.

The two closed-loop control algorithms proceed in three steps: acquisition of the unsteady pressure signal, processing of the control signal by the control algorithm in real-time and then sending of the resulting signal to drive the DDV valve. The algorithms have been implemented on a 32-bit M62 digital signal processing (DSP) board, developed by Innovative Integration, based on the Texas Instruments TMS320C6201 processor.

Unsteady measurements of pressures, light and valve displacements are recorded on a PC-based data acquisition system incorporating a sixteen-channel PCI-MIO-16XE-10 acquisition board from National Instruments. The signals are conditioned using an isolation amplifier and an eighth-order elliptic low-pass filter. The cut-off frequency is automatically set to one-third of the sampling rate (5 *kHz*). The SPL data presented are acquired over periods of up to 20 seconds and averaged over the maximum number of 1 second frames available.

Actuation for control was achieved using the same high frequency servo valve described in Section 2.1.2 (DDV valve from Moog) to modulate the fuel flow rate into the swirler and hence produce variations in equivalence ratio in the premix ducts as shown in the fuel system schematic (Figure 4-3). The DDV uses a linear force motor where the stroke is proportional to

the applied voltage. The large pressure drop across the regulator and the inertia of the flow meter means that the mass flow rate is effectively constant upstream of the plenum, in spite of the high frequency modulations downstream. The plenum provides mass storage, so that the fuel flow rate through the DDV can change as its open area is modulated. The pipe length between the DDV and the swirler unit was kept as short as possible in order to decrease the attenuation and time delay. Note that there is a significant time delay in the actuation due to the transport of the fuel from the location to the burning one since that needs to be accounted for in the control strategy.

4.2 Combustor Dynamics

4.2.1 Self-excited oscillations

The instability characteristics of the rig have been investigated for a range of flow conditions and plenum and combustor lengths. Within the typical envelope of the operating parameters (m_a=0.03-0.08 *kg/s*, ϕ=0.5-1.0) several intense combustion instabilities with multiple frequencies have been observed. Typical pressure spectra contain dominant peaks at one or two low frequencies (100 - 300 *Hz*) and an additional high frequency peak (550 - 700 *Hz*). These frequencies relate approximately to half-wavelength modes of the plenum and to quarter wavelength modes of the combustor.

In the current set of feedback control tests, the experimental data has been obtained in the ranges m_a=0.03-0.05 *kg/s* and m_f=1.6-2.5 *g/s*, resulting in ϕ=0.5-0.75. For the geometric configuration shown in Figure 4-1 (L_p=1.73 m., L_c=1.0 m.) the rig exhibits a 207 *Hz* plenum mode instability. In order to obtain different unstable frequencies the plenum length was varied (L_p=1.46/1.73/1.97 *m.*). The pressure spectra for these cases all contain dominant low frequency peaks (<300 *Hz*) with magnitudes of up to 165 *dB* that set an ideal challenge for active control (Figure 4-4).

These dominant modes correspond to the second harmonic of the plenum (wavelength=L_p). The fundamental and the higher harmonics are also present. In addition, for the L_p=1.97 *m* case

there is a peak at 244 *Hz* which corresponds to the quarter wavelength mode of the combustor tube. The appearance of the combustor modes is not as predictable as the plenum modes.

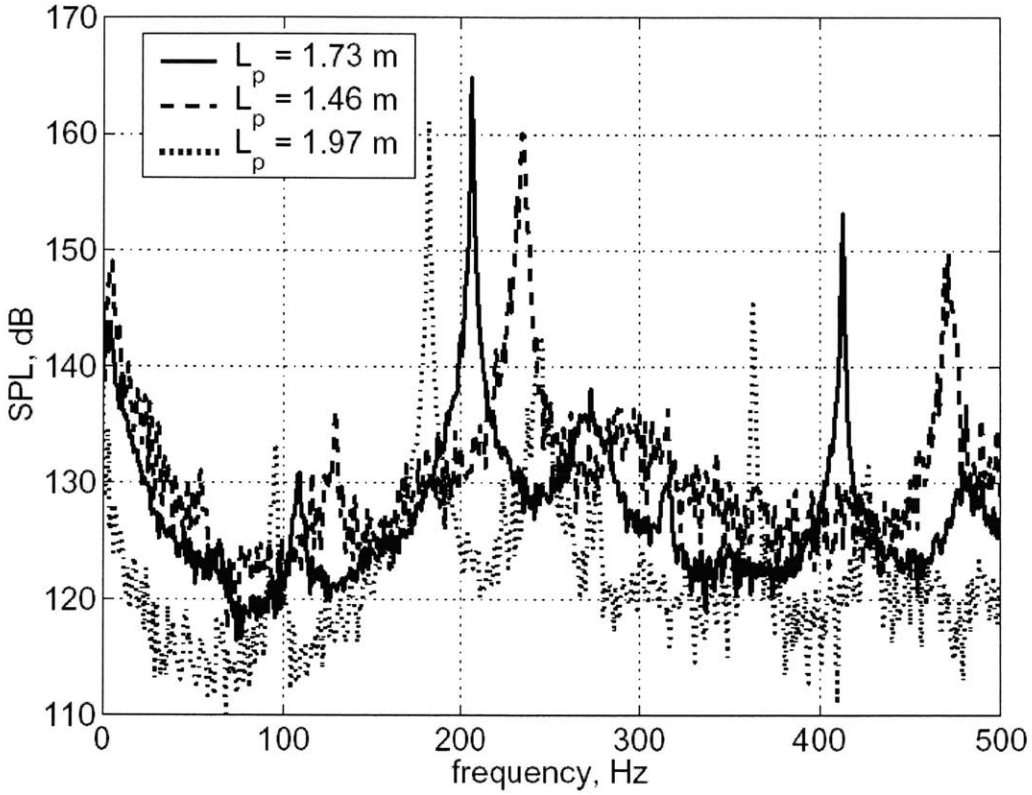

Figure 4-4 SPL spectrum of the self-excited combustion oscillations; m_a=0.04 *kg/s*, ϕ=0.7.

4.2.2 Determination of τ_{tot}

The total time delay, τ_{tot}, is needed to determine the adaptation law in Eq.(3-4) and n, respectively. This can be determined through open-loop forcing and investigating the transfer function $G_p(s) = p'/V$ at a range of frequencies through system-identification tests [18]. At the desired operating condition, a simple phase shift controller was applied in order to minimize the self-excited oscillation. In addition to this, a sine sweep of V(t), with changing frequency from 40 *Hz* to 430 *Hz*, was also supplied to the DDV valve. The resulting pressure data was post processed with a bandpass filter [80 *Hz* – 230 *Hz*] to better capture dynamics around the unstable frequency. $G_p(s)$ was obtained using a linear ARX model-structure [55] and τ_{tot} was found to be 9.6 *msec*.

Initial tests with the Posicast were conducted using a system-identification reduced order model to obtain optimal starting values for the control parameters. To obtain this another system-identification was carried out using $V(t-\tau_{tot})$ and $p'(t)$ to yield an ARX model, which resulted in a $G_p(s)$ given by

$$G_p(s) = -0.8787 \frac{s^3 + 1071s^2 + 2.105 \cdot 10^6 s + 7.894 \cdot 10^6}{s^4 + 24.75s^3 + 2.366 \cdot 10^6 s^2 + 3.312 \cdot 10^7 s + 1.169 \cdot 10^{12}} e^{-0.0096s}$$

where $sign(k_0) = -1$. This negative high frequency gain was an unexpected result and might be the result of additional dynamics in the fuel supply system that were not addressed in the model.

For the current tests the sign of k_0 was changed in the adaptation scheme. In the current tests, the user inputs into the adaptive Posicast were a sampling rate of 2 *kHz*, n=19, a=Z_c=1000, γ_1=γ_2=100,000 and γ_3=10, unless otherwise stated.

4.3 Closedloop Control Results

(Nominal Case- L_p=1.73 m)

Initial tests of the controller produced reductions in noise that were 5-15 *dB* larger than those gained with the appropriately tuned fixed phase shift controller. However, the intermittent presence of a low frequency mode of the order of 1 *Hz* degraded the performance. Figure 4-5 shows a typical time series indicating the presence of the low frequency mode when the controller is on.

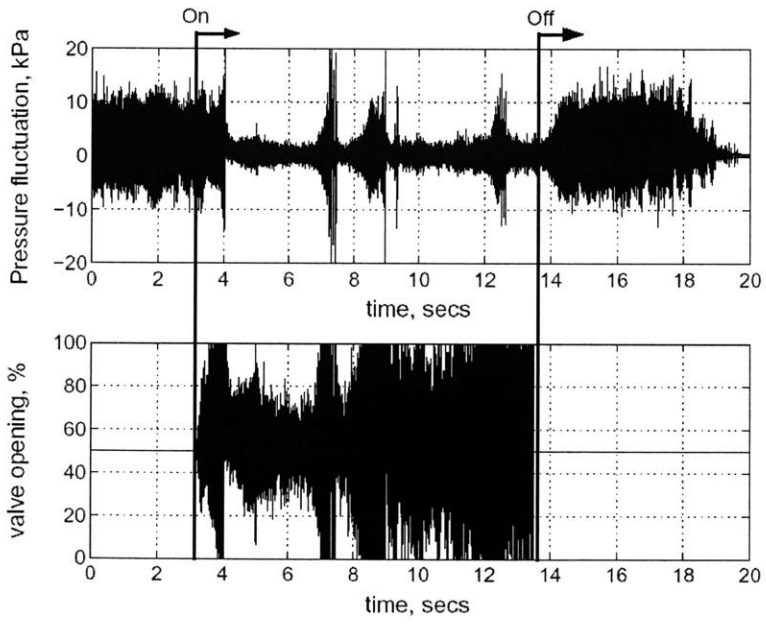

Figure 4-5 Time series showing the low frequency fluctuations present in the combustor when the adaptive Posicast controller is activated; m_a=0.04 *kg/s*, ϕ=0.65, τ_{tot}=9.6 *ms*, L_p=1.73 *m*, zero initial conditions for control parameters.

Analysis of the valve time series suggested that there was significant control action around 100 *Hz*, once the main instability was stabilized, prior to the controller divergence. A bandpass filter (120-500 *Hz*) was introduced between detection and the controller input to remove the low frequency dynamics. Figure 4-6 shows the resulting improvement in performance. The controller is turned on at 4.4 seconds and stabilization is achieved in about 3.6 seconds. The control parameters such as k_1 and k_2 start at zero and converge to a specific value, as shown for k_1 in Figure 4-6. The zero initial conditions simply imply that the controller does not know the combustion dynamics initially and these values are automatically tuned by the adaptive controller to give optimal performance. However, it should be mentioned that the settling time for other test cases, under nominally the same operating conditions, can be large (up to 7 seconds). This was due to two reasons; 1) higher pressure oscillations (more than 10 *kPa*) made the valve saturate (already present to some degree in Figure 4-6) and 2) zero initial conditions of the control parameters requires time for the controller to search for the optimal control parameters. When the pressure amplitude was smaller than 10 *kPa* and the initial conditions were chosen based on $G_p(s)$, the settling time could be reduced to less than 1 second as shown in Figure 4-7. Figure 4-8 shows typical pressure spectrum for the control on/off cases where there is a reduction of approximately 15 *dB* by the phase shift controller and 30 *dB* for the adaptive Posicast controller at the 207 *Hz* instability[1]. One of the reasons for the limited performance of the delay controller was due to a low frequency mode, which can be seen in Figure 4-8 and is similar to that seen in Figure 4-5. In some cases, when this low frequency mode was not present, the phase shift controller was able to reduce pressure oscillations up to 26 *dB*.

[1] Note: all pressure spectra presented are for pre-filtered data

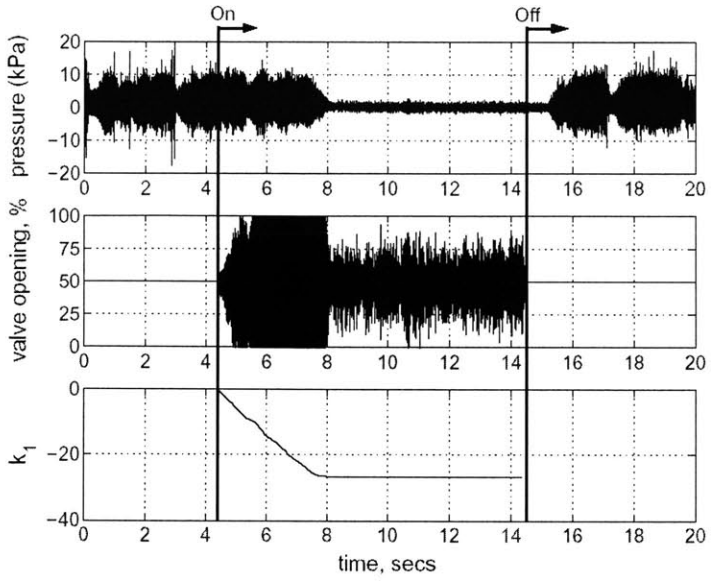

Figure 4-6 Time series showing the improvement on the pressure fluctuations in the combustor gained by filtering the adaptive Posicast controller input; m_a=0.04 *kg/s*, ϕ=0.65, τ_{tot}=9.6 *ms*, L_p=1.73 *m*, controller input filter=120-500 *Hz*.

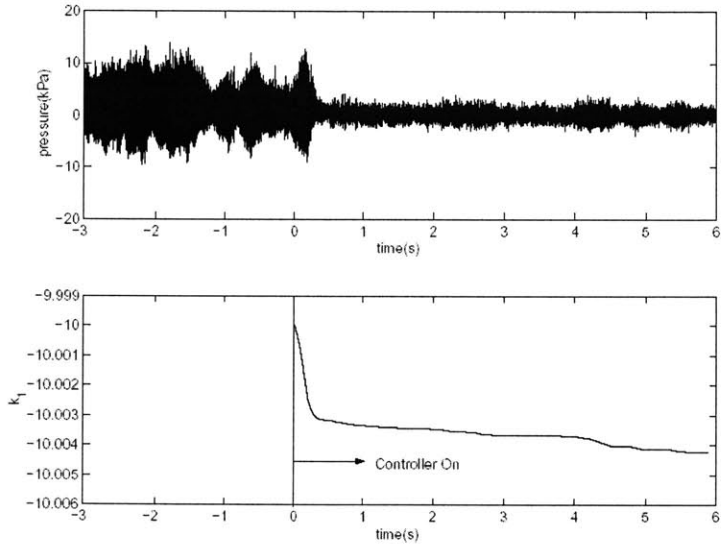

Figure 4-7 Time series showing the improvement in the settling time of the adaptive Posicast controller when appropriate initial conditions are chosen; m_a=0.04 *kg/s*, ϕ=0.65, τ_{tot}=9.6 *ms*, L_p=1.73 *m*, initial conditions of k_1=-10, k_2=10.

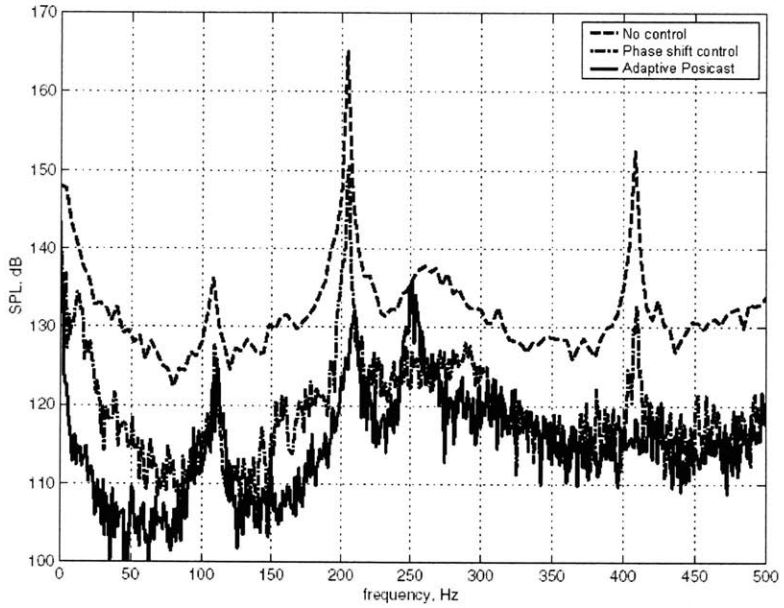

Figure 4-8 SPL spectra showing the reduction in noise when the adaptive Posicast and the phase shift controllers are turned on; m_a=0.04 *kg/s*, ϕ=0.65, τ_{tot}=9.6 *ms*, L_p=1.73 *m*, controller input filter=120-500 Hz.

4.4 Robustness Studies

As mentioned previously, the adaptive Posicast controller can automatically tune its control parameters when the combustion dynamics change. In this section, I carry out extensive robustness studies with respect to changes in the resonant frequency, total time delays, changes in operating conditions and initial conditions of control parameters.

4.4.1 Changes in the Resonant Frequency

The resonant frequency varies as the temperature of a combustor changes. Banaszuk *et al.* [56] reported a 20% change in resonant frequency over a 9 second period during warming up of an experimental combustor. As a result, at a start up or during thrust change, the controller needs to be able to cope with possible changes in frequency. As explained in Section 4.2.1, the resonant frequency was changed by changing the plenum length, L_p. Initially, L_p was changed from 1.73 to 1.46 *m* and both the delay and the Posicast controllers were tested with parameters predetermined in the nominal case (L_p=1.73 m). Figure 4-9 shows the pressure spectrum and as expected, the resonant frequency moved to 240 *Hz*. The controller produced a 28 *dB* reduction at the unstable frequency. It is worth noting that k_1 converges to positive values for this case as shown in Figure 4-10, whereas it converges to a negative value in the nominal case in Figure 4-6. The phase shift controller, using time delay/gain inputs determined in the nominal case, did not have any effect and has not been included in Figure 4-10.

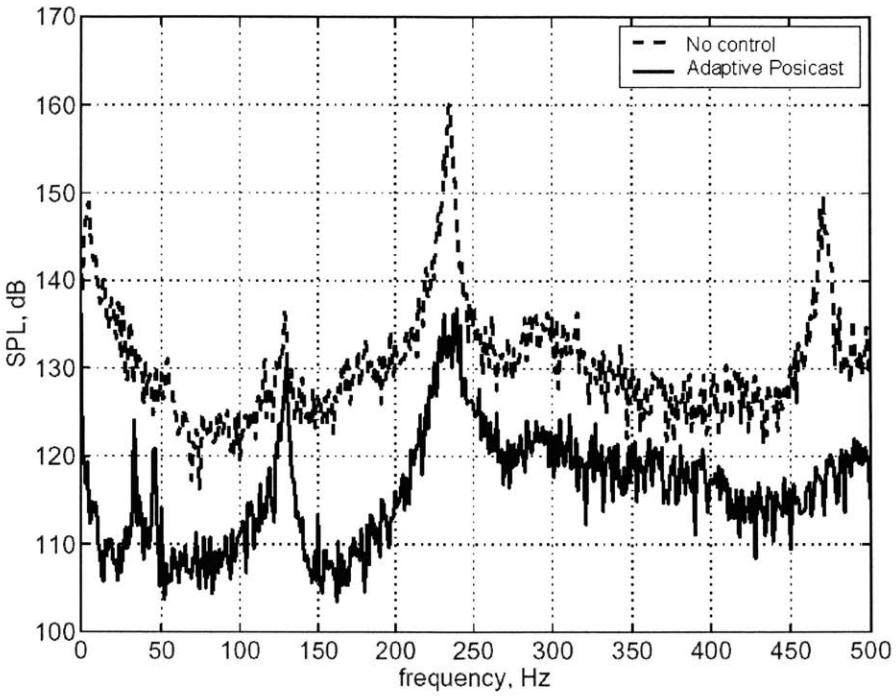

Figure 4-9 SPL spectra showing the reduction in noise when the Posicast is turned on in the shorter plenum case; m_a=0.04 kg/s, ϕ=0.70, τ_{tot}=9.6 ms, L_p=1.46 m, controller input filter=120-500 Hz.

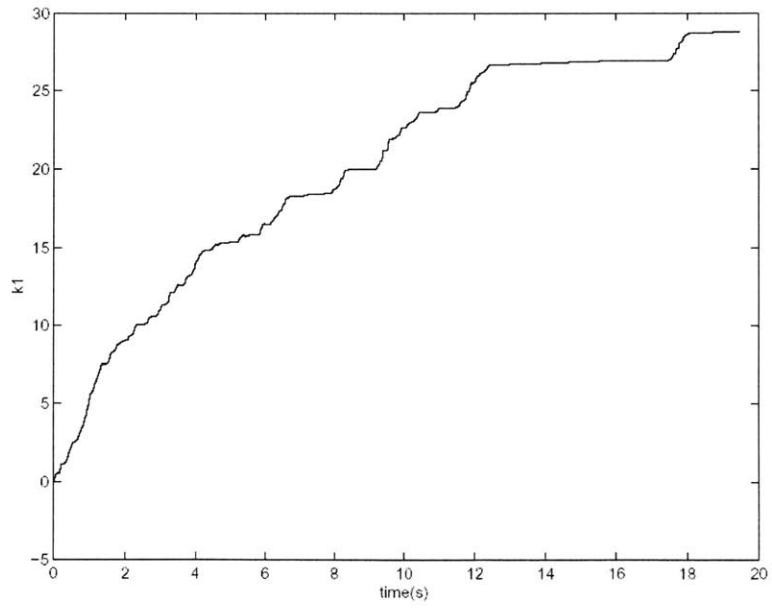

Figure 4-10 Change of the controller parameter, k_1 in case of Figure 4-9; m_a=0.04 kg/s, ϕ=0.70, τ_{tot}=9.6 ms, L_p=1.46 m, zero initial conditions for control parameters.

Next, L_p was increased to 1.97 *m*, and the phase shift and the adaptive Posicast controllers were tested with parameters predetermined in the nominal case. Once again the phase shift controller had no significant effect. Figure 4-11 shows the pressure spectrum without control and with the adaptive Posicast cases and interestingly, two modes at 180 and 244 *Hz* were observed in the no control case. The latter is the quarter wavelength mode for the combustor tube. The optimal k_1 values are different for these two modes and hence k_1 is found to oscillate as it tries to control first one and then the other mode (Figure 4-12). Finally, k_1 converges to a value that is in between these two optimal values (Note: average k_1 negative in this case). Large adaptation gains may generate overshoot during convergence, but this can be reduced using a smaller adaptation gain, γ_1. When the adaptation gain was halved to γ_1=50000, k_1 showed less oscillatory behavior (Figure 4-12) and the resulting pressure reduction was 15 *dB* (4 *dB* lower that that achieved with γ_1=100000).

For both cases described above, the performance of the phase shift controller could be improved by optimizing the time delay input. However, for L_p=1.46 *m*. only a 7 *dB* reduction was achieved, compared with 28 *dB* for the adaptive Posicast. For L_p=1.97 *m*., a 22 *dB* reduction was achieved, compared with only 15 *dB* for the adaptive Posicast. In this case, though, there was also a 10 *dB* increase at the fundamental

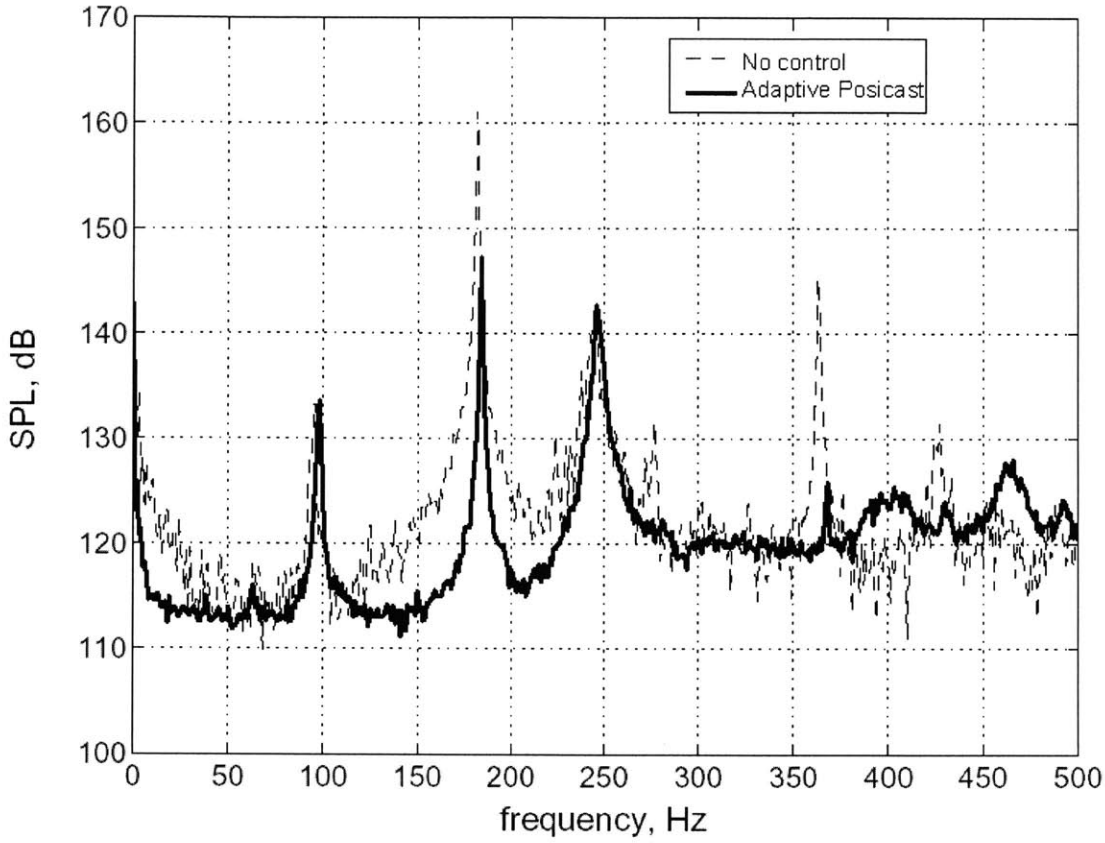

Figure 4-11 SPL spectra showing the reduction in noise when the adaptive Posicast is turned on in the longer plenum case; m_a=0.04 *kg/s*, ϕ=0.65, τ_{tot}=9.6 *ms*, L_p=1.97 *m*

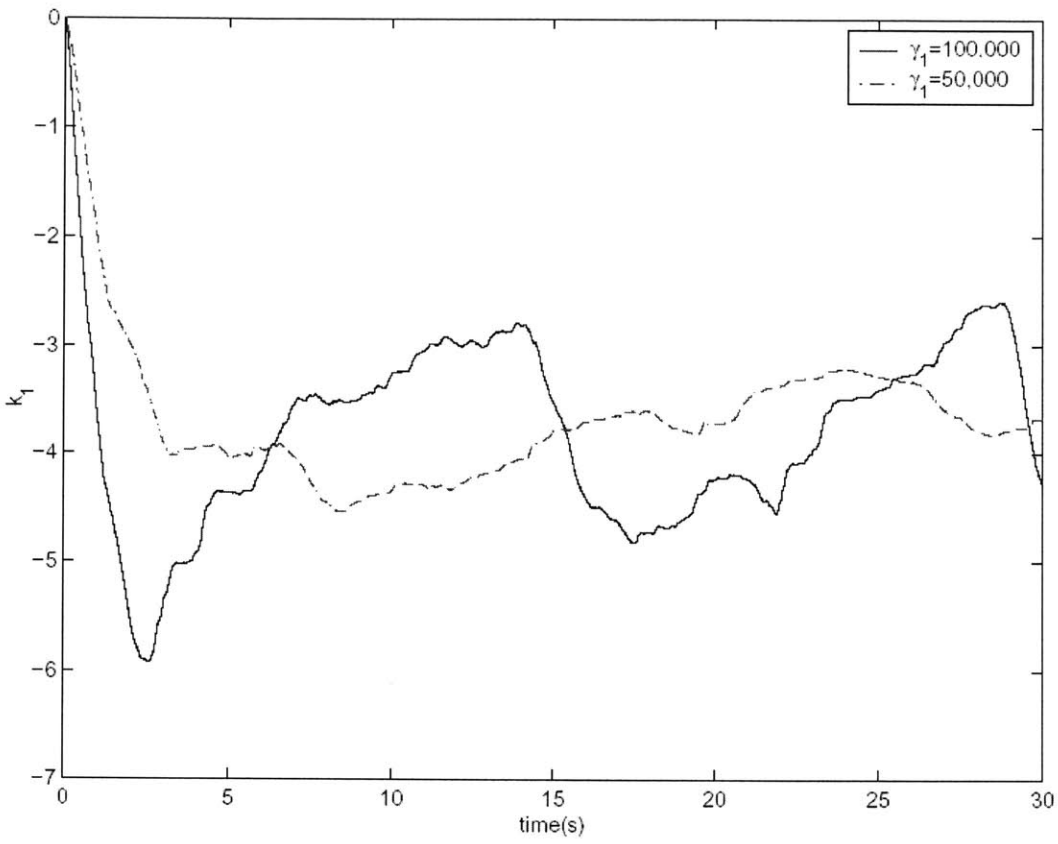

Figure 4-12 Change of the controller parameter, k_1 in a longer plenum case with different adaptation gain, γ_1 ; m_a=0.04 *kg/s*, ϕ=0.65, τ_{tot}=9.6 *ms*, L_p=1.97 *m*.

4.4.2 Variation in total time delay

The impact of a change in the total time delay on the performance of the adaptive Posicast controller was also evaluated. Such a change can occur with a change in the flow rate or a change of the burning zone location. Instead of changing the operating conditions, the total time delay in the Posicast was changed by τ_Δ. Experimental results show that the controller still maintains control up to a maximum of τ_Δ=1.1msec less than the τ_{tot} derived from the system

identification, as shown in Figure 4-13. However, control was lost if τ_{tot} was increased beyond 9.6 ms.

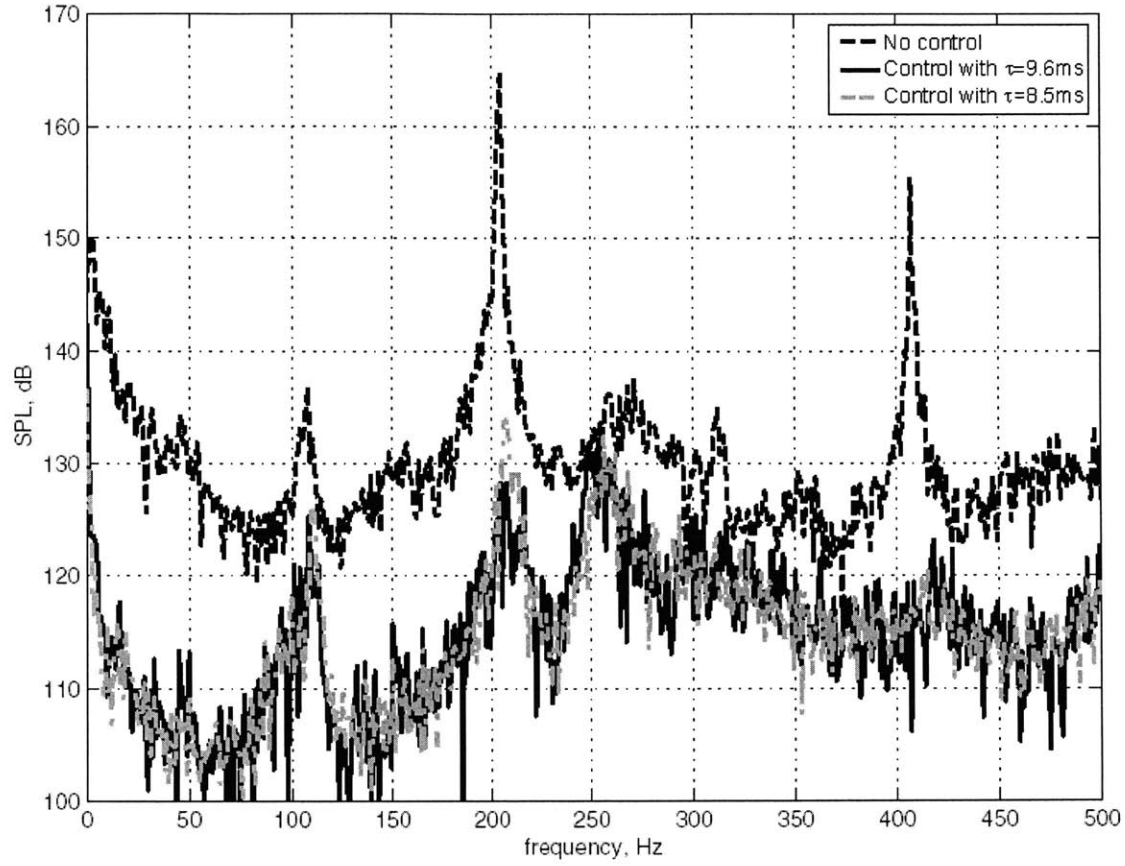

Figure 4-13 SPL spectra showing the reduction in noise when the adaptive Posicast was used with correct(τ_{tot}=9.6*ms*) and incorrect time delay (τ_{tot}=8.5*ms*); m_a=0.04 *kg/s*, ϕ=0.7, τ_{tot}=9.6 ms, L_p=1.73 *m*, controller input filter=120-500 *Hz*.

4.4.3 Changes in flow rate and equivalence ratio

The robustness of the adaptive Posicast controller was investigated with respect to changes in the mass flow rate of the air. The controller was turned on at the nominal case with an air flow rate of 0.04 *kg/s*, which was then decreased slowly by 23% (0.009 *kg/s*) over 100 seconds while keeping the equivalence ratio constant. Figure 4-14 shows that the controller was able to

maintain control as the flow rate changes. After 100 seconds, once the controller was turned off, the pressure amplitude returned to previous levels indicating that the final operating condition was also unstable. The air mass flow rate was also increased from 0.04 *kg/s* to 0.055 *kg/s*. However, at higher air flow rate, the combustion was stable.

The rig exhibits an unstable mode at 207 *Hz* when ϕ=0.6-0.7, and ϕ=0.6 is very close to the flammability limit. The controller maintains control as ϕ is varied within this range. At ϕ larger than 0.75, a combustor tube mode above 600 *Hz* was excited. As a result, the controller can only be tested in the range ϕ=0.6-0.7 due to bandwidth limitation of the DDV valve and the flammability limit.

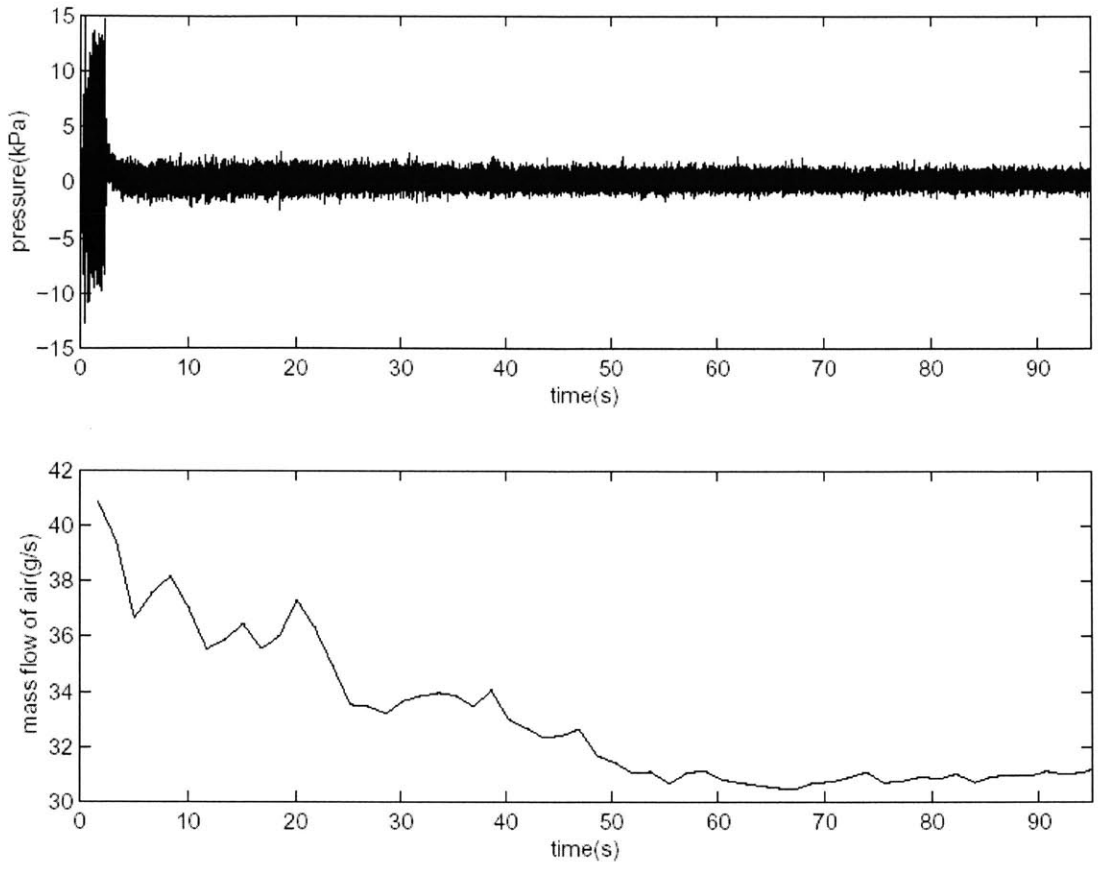

Figure 4-14 Time series showing the effect of the adaptive Posicast controller with changes in the mass flow rate of air; m_a=0.04 *kg/s*, ϕ=0.7, L_p=1.73 *m*, controller input filter=120-500 *Hz*.

4.4.4 Initial Conditions of the Control Parameters

As mentioned earlier, carefully chosen initial conditions can reduce the settling time of the adaptive Posicast controller significantly. We can also test the sensitivity of the controller to the initial conditions of control parameters, by deliberately setting the control parameters far from the optimum values. The control gain, k_1, was set to +10 initially, which is opposite in sign to the optimal value. Figure 4-15 shows that the controller still converges to the optimal parameters and that it is robust with respect to the initial conditions of the control parameters. However, the

settling time increased by an order of magnitude over that shown in Figure 4-15 where the initial condition of k_1 is set close to the optimal value.

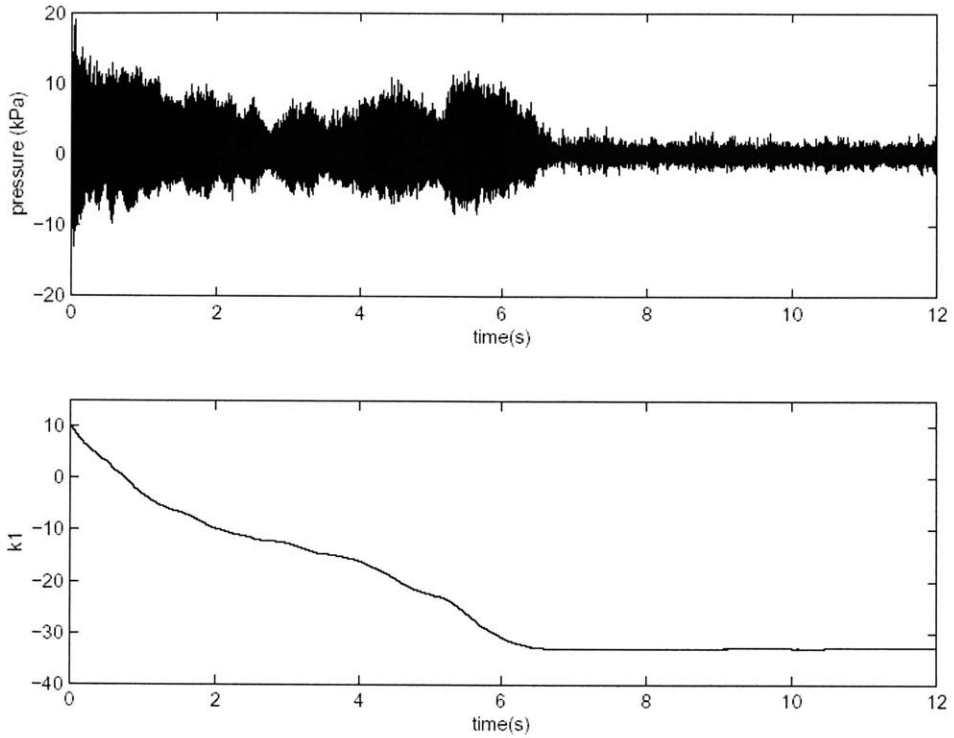

Figure 4-15 Time series showing the effect of the adaptive Posicast controller with incorrect initial condition in the control parameter; m_a=0.04 *kg/s*, ϕ=0.65, τ_{tot} =9.6 *ms*, L_p=1.73 *m*, controller input filter=120-500 *Hz*.

4.5 Summary

Forced unsteady combustion has been successfully achieved by using a high frequency valve to modulate the rate of fuel injection into a Rolls Royce RB211-DLE swirler unit. Tests on the current combustion rig, which has a significant time delay (9.6 *ms*), have shown that it can successfully reduce noise levels by an additional 5-15 *dB* compared to a tuned fixed phase shift controller and by pulsing the same amount of fuel (2%). Better performance of the Posicast controller in a nominal condition can be attributed as follows: 1) Since the closed loop is essentially a delay free system due to the design of the adaptive Posicast, the transport delay does not interact with the inherent dynamics of the combustor. Hence, it is not likely to introduce secondary peaks. 2) Due to 1), larger gain is permitted which results in larger pressure reduction at the unstable frequency without generating secondary peaks.

Robustness studies have been started to test the adaptive Posicast controller over a wide range of frequencies and operating conditions. The initial results have been encouraging. With changes in the resonant frequency of 20%, the adaptive Posicast controller was able to adjust its control parameters and produce a significant pressure reduction. Even with two unstable modes, the controller adjusted its parameters to compromise and produce a pressure reduction in both modes. The algorithm is not currently capable of adapting to a variable τ_{tot}, however 1.1msec delay change was achievable. For air flow rate and equivalence ratio, 23% and 14% changes, respectively, were allowable.

Due to limited authority of the actuator and no prior knowledge of combustion dynamics (zero initial conditions of control parameters), the settling time could be large (up to 7 seconds). Also, when two unstable modes are present, large adaptation gain produced overshoot in control parameters. These suggest that adaptation gain and initial conditions of control parameters need to be selected carefully to make the adaptive Posicast controller better perform in the 'transient region'. After the control parameters were converged, the performance of the controller was not changed with changes in the adaptation gain and the initial conditions.

5. Conclusions

This thesis addressed current challenges in the area of combustion control in three distinct directions for transition of the active control strategy to industrial applications. First developing an understanding of the interactions between hydrodynamics and heat release dynamics and their impact on the underlying acoustics in the combustion system. Secondly addressing the optimization of emissions and other burning characteristics in addition to controlling the instabilities in a combustor. Thirdly verifying the active control strategy at more realistic conditions including swirl, a large convective time delay in the control input and changes in the resonant frequency and operating conditions. I addressed these challenges in three different combustor configurations, each with unique characteristics.

In Chapter 2, I addressed emission reduction in addition to instability suppression in the premixed backward-facing step combustor (Configuration I) using a transverse air jet near the step. First, a parametric study was conducted to investigate the responsible mechanism for combustion instability. Results showed the impact of fuel/air mixture inhomogeneity is negligible and the hydrodynamics is the dominant mechanism for combustion instability. For this reason, I focused the control effort on modifying the flame-vortex interactions in the combustion zone using a transverse air jet. I studied experimentally the impact of static and modulated transverse jet on stability and emissions. With sufficient momentum, a static air jet injected perpendicular to the incoming flow near the step favorably modified flame-vortex interactions and reduced pressure oscillations by up to 14 *dB*, while reducing NOx emission by an order of

magnitude. Using closed-loop control with pressure feedback, the air jet achieved the same level of pressure reduction with 50% of the air flow rate required in the static air jet case. However, control effectiveness was strongly dependent on the phase angle. Adding small amounts of H_2 either in the air jet or in the primary fuel led to further reduction in OASPL and extension of the flammability limit.

In Chapter 3, I investigated a sensing technology capable of capturing the spatial properties of the combustion zone in the axisymmetric dump combustor (Configuration II). A linear photodiode array which can capture high speed spatio-temporal heat release fluctuations was tested as a feedback sensor in a dump combustor. Pressure measurements identified strong oscillations at 38 *Hz*, the quarter-wave acoustic mode of the inlet tube. Images taken using the linear photodiode array and a Schlieren system showed large-scale flame oscillations due to strong flame-vortex interactions at 38 *Hz*. To develop a model of this combustion system, Proper Orthogonal Decomposition (POD) was used to systematically extract the most energetic modes with the first and second POD modes capturing about 60 and 30% of the total fluctuations, respectively. The first mode was used as a basis function for a System Identification based model. A model-based controller was used for pressure stabilization, which resulted in pressure reduction of up to 23 *dB*. Heat release characteristics, determined using CH* emission, showed that the maximum value of CH* is doubled due to the action of control, and the burning zone moved closer to the step.

Finally, to validate the model-based active control strategy in industrial gas turbine combustion, a Rolls-Royce RB211-DLE industrial gas turbine (Configuration III) was used in Chapter 4. The combustor exhibited a significant time delay (9.6*msec*) in the control input due to

the location of the fuel injection. To accommodate this time delay, the adaptive Posicast controller was used. Tests showed that it could successfully reduce noise levels 5-15 *dB* beyond the level achieved by a phase-shift controller while pulsing the same amount of fuel. Robustness studies showed that the adaptive Posicast controller could also accommodate changes in the combustion dynamics by appropriately tuning its control parameters automatically.

Results obtained from these three configurations show that through an understanding of the underlying physics and reduced-order modeling, one can design an appropriate actuation, sensing and control algorithm, all of which lead to model-based active control that reduces pressure oscillations to background noise. In addition, active control improves other performance matrices, such as reduction in NOx emissions, increase in the volumetric heat release and the extension of the flammability limit, providing key building blocks for transition of the active control technology from laboratories to large-scale applications in propulsion and power generation.

References

[1] J.W.S. Rayleigh, "The theory of Sound", Volume 2, Dover, New York, 1945.

[2] J. R. Hibshman, J. M. Cohen, A. Banaszuk, T. J. Anderson and H. A. Alholm, " Active control of combustion instability in a liquid-fueled sector combustor," *44th ASME Gas Turbine and Aeroengine Technical Congress*, Indianapolis, IN , June 7-10, 1999.

[3] T. Poinsot, F. Bouriennem S. Candel and E. Esposito, "Suppression of combustion instabilities by active control," *Journal of Propulsion and Power*, Vol. 5, No.1 ,pp.14-20, 1989.

[4] S. Park "Modeling of combustion instability at different damkohler conditions," M.S. Thesis, Department of Mechanical Engineering, MIT, 2001.

[5] M. Fleifil, A. M. Annaswamy, Z. Ghoniem and A. F. Ghoniem, "Response of a laminar premixed flame to flow oscillations: A kinematic model and thermoacoustic instability results," *Combustion and Flame*, Vol. 106, p.487-510, 1996.

[6] S. Park, A.M. Annaswamy and A.F. Ghoniem, "Heat release dynamics modeling of kinetically controlled burning," *Combustion and Flame*, Vol.128, pp.217-231, 2002.

[7] K. Yu, K.J. Wilson and K.C. Schadow, "Scale-up experiments on liquid-fueled active combustion control," AIAA Paper 98-3211, *34th AIAA/ASME/SAE/ASEE Joint Propulsion Conference & Exhibit*, Cleveland, OH, 1998.

[8] E. Gutmark, T.P. Parr, K.J. Wilson, D.M. Hanson-Parr and K.C. Schadow, "Closed-loop control in a flame and a dump combustor," *IEEE Control Systems*, Vol. 13, pp.73-78, 1993.

[9] P. J. Langhorne, A.P. Dowling and N. Hooper, "Practical active control system for combustion oscillations," *Journal of Propulsion and Power* vol.6, No. 3, pp324-333, 1990.

[10] V. Yang, A. Sinha and Y-T Fung, "State-feedback control of longitudinal combustion instabilities," *Journal of Propulsion and Power,* Vol.8, No. 1, pp. 66-73, 1992.

[11] J. P. Hathout, A. M. Annaswamy, M. Fleifil and A. F. Ghoniem, "A model-based active control design for thermoacoustic instability," *Combustion Science and Technology,* Vol. 132, pp. 99-138, 1998.

[12] A.M. Annaswamy, M. Fleifil, J.W. Rumsey, R. Prasanth, J.P. Hathout and A.F. Ghoniem, "Thermoacoustic instability: model-based optimal control designs and experimental validation," *IEEE Transactions on Control Systems Technology*, Vol. 8, No. 6, November 2000.

[13] P. Mehta, A. Banaszuk, M. Soteriou and I. Mezic, "Fuel control of a ducted bluffbody flame," *42nd Conference on Decision and Control*, Maui, Hawaii, December 2003.

[14] G.A. Richards, G. J. Morris, D. W. Shaw, S. A. Keeley and M. J. Welter, "Thermal pulse combustion," *Combustion Science and Technology*, Vol. 94, pp.57-85, 1993.

[15] T. Lieuwen, Y. Neumeier and B. T. Zinn, "The role of unmixedness and chemical kinetics in driving combustion instabilities in lean premixed combustors," *Combustion Science and Technology*, Vol. 135, pp.193-211, 1998.

[16] S. Park, A. M. Annaswamy and A. F. Ghoniem, "A model-based self-tuning controller for kinetically controlled combustion instability," *American Control Conference*, Anchorage, Alaska, USA, May 8-10, 2002.

[17] B.J Brunell. "A system identification approach to active control of thermoacoustic instability," M.S. Thesis, Department of Mechanical Engineering, MIT, 2000.

[18] S. Murugappan, S. Park, A.M. Annaswamy, A.F. Ghoniem, S. Acharya and D.C. Allgood, "Optimal control of a swirl stabilized spray combustor using system identification approach," *Combustion Science and Technology* , Vol.175, pp.55-81, 2003.

[19] Y. Neumeier, N. Markopoulos and B.T. Zinn, "A procedure for real-time mode decomposition, observation and prediction for active control of combustion instabilities," *In Proceedings of the IEEE Conference on Control Applications*, paper No. 97318, Hartford, CT, 1997.

[20] A. Banaszuk, Y. Zhang and C. A. Jacobson. "Adaptive control of combustion instability using extremum-seeking," *American Control Conference*, Chicago, IL, 2000.

[21] J.P. Hathout, M. Fleifil, A.M. Annaswamy and A.F. Ghoniem, "Combustion instability and active control using periodic fuel injection," *AIAA Journal of Propulsion and Power*, Vol. 18, No. 2, pp.390 -399, March-April 2002.

[22] S. Evesque, A.P. Dowling and A.M. Annaswamy, "Self-tuning regulators for combustion oscillations," *Royal Society Journal Proceedings of the Mathematical, Physical and Engineering Sciences*, Vol. 459, Issue 2035, pp 1709-1749, 2003.

[23] J. M. Cohen and T. J. Anderson, "Experimental investigation of near-blowout instabilities in a lean premixed step combustor," AIAA 96-0819, *34th Aerospace Sciences Meeting and Exhibit*, 1996.

[24] C. O. Paschereit, W. Weisenstein and E. Gutmark, "Role of coherent structures in acoustic combustion control," *AIAA 98-2433, 29th AIAA Fluid Dynamics Conference*, 1998.

[25] K.C. Schadow, E. Gutmark, K.J. Wilson and R.A.Smith, "Multistep dump combustor design to reduce combustion instabilities," *Journal of Propulsion and Power*, Vol. 6, No. 4, pp.407-411, 1990.

[26] J.-Y. Ren, W. Qin, F. N. Egolfopoulos and T.T. Tsotsis, "Strain-rate effects on hydrogen-enhanced lean premixed combustion," *Combustion and Flame*, Vol.124, pp.717-720, 2001.

[27] R. W. Schefer, "Hydrogen enrichment for improved lean flame stability," *International Journal of Hydrogen Energy*, Vol.23, pp.1131-1141, 2003.

[28] G.S. Jackson, R. Sai, J.M. Plaia, C.M. Boggs, K.T. Kiger, "Influence of H_2 on the response of lean premixed CH_4 flames to high strained flows," *Combustion and Flame*, Vol.132, pp.503-511, 2003.

[29] G. J. Rortveit, K. Zepter, O. Skreiberg, M Fossum, J. E. Hustad, "A comparison of low-NOx burners for combustion of methane and hydrogen mixtures," *Proceedings of the Combustion Institute* Vol.29, pp. 1123-1129. 2002.

[30] J.R. Maughan, J.H. Bowen, D.H. Cooke and J.J. Tuzcon, "Reducing gas turbine emissions through hydrogen-enhanced steam-injected combustion," *Journal of Engineering for Gas Turbines and Power*, Vol.118, pp. 78-85, 1996.

[31] J.L. Gauducheau, B. Denet, G. Searby, "A numerical study of lean CH_4/H_2/air premixed flames at high pressure," *Combustion Science and Technology*, Vol.137, pp. 81-99, 1998.

[32] A.J. Riley, S. Park, A.P. Dowling, S. Evesque and A.M. Annaswamy, "Adaptive closed-loop control on an atmospheric gaseous lean-premixed combustor," *ASME IGTI Turbo Expo*, Atlanta, GA, June 2003.

[33] B. Higgins, M. Q. McQuay, F. Lacas and S. Candel, "An experimental study on the effect of pressure and strain rate on CH chemiluminescence of premixed fuel-lean methane/air flames," *Fuel* 80, pp. 1583-1591, 2001.

[34] B. D. Bellows, Q. Zhang, Y. Neumeier, T. Lieuwen, and B. T. Zinn, "Forced response studies of a premized flame to flow disturbances in a gas turbine combustor," *41st AIAA Aerospace Sciences Meeting and Exhibit*, Reno, NV, January 2003.

[35] J. G. Lee, K. Kim, and D. A. Santavicca, "Measurement of equivalence ratio fluctuations and its effect on heat release during unstable combustion," *Proceedings of the Combustion Institute*, Vol. 28, 2000.

[36] J. M. Cohen, J. H. Stufflebeam, and W. Proscia, "The effect of fuel/air mixing on actuation authority in an active combustion instability control system," *2000-GT-0083 Proceedings of ASME TURBOEXPO 2000*, Munich, Germany, May, 2000.

[37] J. Brouwer, B. A. Ault, J. E. Bobrow, and G. S. Samuelsen, "Active control for gas turbine combustors," *23rd Symposium (International) on Combustion/The Combustion Institute*, pp. 1087-1092, 1990.

[38] T. Lieuwen, H. Torres, C. Johnson and B.T. Zinn, "A mechanism of combustion instability in lean premixed gas turbine combustors," *Journal of Engineering for Gas Turbine and Power,* Vol. 123, No. 1, pp. 182-189, 2001.

[39] K.K. Venkataraman, L.H. Preston, D.W. Simons, B.J. Lee, J.G. Lee, D.A. Santavicca, "Mechanism of combustion instability in a lean premixed dump combustor," *Journal of Propulsion and Power*, Vol.15, No.6, pp.909-918, 1999.

[40] H. Najm and A. F. Ghoniem, "Modeling pulsating combustion due to flow-flame interactions in vortex-stabilized pre-mixed flames," *Combustion Science and Technology*, Vol. 94, pp.259-278, 1993.

[41] S. H. Smith and M. G. Mungal, "Mixing, structure and scaling of the jet in crossflow," *Journal of Fluid Mechanics*, Vol. 357, pp. 83-122, 1998

[42] K. Hanamura, K. Bohda and Y. Miyairi, "A study of super-adiabatic combustion engine," *Energy Conversion and Management,* Vol. 38, No. 10-13, pp.1259-1266, 1997.

[43] A.F. Ghoniem, A.M. Annaswamy, S. Park, Z. C. Sobhani, "Stability and emissions control using air injection and H2 addition in premixed combustion," *Proceedings of the Combustion Institute*, Vol. 30, 2004.

[44] P. Holmes, J. Lumley and G. Berkooz, Turbulence, Coherent Structures, Dynamical Systems and Symmetry, Cambridge University Press, 1996.

[45] S. Murugappan, S. Park, A. M. Annaswamy, A. F. Ghoniem, S. Acharya, and D. C. Allgood, "Optimal control of a swirl stabilized spray combustor using system identification approach," *Combustion Science and Technology,* vol. 175, pp. 55-81, 2003.

[46] S. Ravindran, "A reduced order approach to optimal control of fluids using proper orthogonal decomposition," *International Journal for Numerical Methods in Fluids*, Vol. 34, pp. 425–448, 2000.

[47] W. R. Graham, J. P. Peraire and K. Y. Tang, "Optimal control of shedding using low order models, Part I- Open-loop model development," *International Journal for Numerical Methods in Engineering*, Vol. 44, pp. 945–972, 1999.

[48] W. R. Graham, J. P. Peraire and K. Y. Tang, "Optimal control of shedding using low order models, Part II- Model-based control," *International Journal for Numerical Methods in Engineering*, Vol.44, pp. 973–990, 1999.

[49] E. Arian, M. Fahl and E. W. Sachs, "Trust-region proper orthogonal decomposition for flow control," *NASA/CR-2000-210124,ICASE Report No. 2000-25*, 2000.

[50] D. Sahoo, S. Park, A. M. Annaswamy and A. F. Ghoniem, "A recursive proper orthogonal decomposition algorithm for real-time tracking of evolving reduced order basis in dynamical systems," *Technical Report, Active-Adaptive control Laboratory*, 2004.

[51] A. Newman, "Model reduction via the Karhunen-Loève expansion," *Technical Research Report, T. R. 96-32 and 96-33*, Institute for Systems Research, University of Maryland, Maryland, USA, 1996.

[52] D. Tang, D. Kholodar, J.-N. Juang and E. H. Dowell, "System identification and proper orthogonal decomposition method applied to unsteady aerodynamics," *AIAA Journal*, Vol.39, 2001.

[53] S. H. Jeong, B. Bienkiewicz. "Application of autoregressive modeling in proper orthogonal decomposition of builing wind pressure," *Journal of Wind Engineering and Industrial Aerodynamics*, 69-71, pp.685-695, 1997.

[54] D. A. Gillies, "Low-dimensional control of the circular cylinder wake," *Journal of Fluid Mechanics*, Vol. 371, pp.157-178, 1998.

[55] L. Ljung, System Identification, second edition, Prentice Hall, Upper Saddle River, NJ, 1999.

[56] A. Banaszuk, Y. Zhang and C. A. Jacobson, "Adaptive control of combustion instability using extremum-seeking," *American Control Conference*, Chicago, USA, 2000.